THESIS

GEOGRAPHICAL ASSESSMENT OF ALGAL PRODUCTIVITY AND WATER INTENSITY ACROSS THE UNITED STATES

Submitted by

David Quiroz

Department of Mechanical Engineering

In partial fulfillment of the requirements

For the Degree of Master of Science

Colorado State University

Fort Collins, Colorado

Summer 2021

Master's Committee:

Advisor: Jason C. Quinn

Anthony Marchese
Kenneth Reardon

ABSTRACT

GEOGRAPHICAL ASSESSMENT OF ALGAL PRODUCTIVITY AND WATER INTENSITY

ACROSS THE UNITED STATES

Water consumption due to evaporation in open algal cultivation systems represents a significant research gap in the resource assessment literature. Existing algal evaporation models often lack high spatiotemporal resolution or are not validated with experimental systems. This study presents a geographical and temporal assessment of the water requirements for commercial-scale production of algae biomass through a dynamic integrated thermal and biological modeling framework. Water demands were calculated through a validated dynamic thermal model which predicts temperature with an accuracy of -0.96 ± 2.72 °C and evaporation losses with a 1.46 ± 5.92 % annual accuracy. The biological model was validated with experimental data representing the current state of technology and shows an average error of -4.59 ± 8.13 %. The integrated thermal growth model was then utilized to simulate the water demands for biomass production of a 400-hectare algae farm at 198 different locations across the United States over a period of 21 years. Simulation outputs were used to determine algal protein yields, based on protein content, and fuel production via hydrothermal liquefaction. This foundation is integrated with life cycle methodology to determine the water footprint of algal biomass, proteins, and biofuels and to compare them to those of traditional energy crops and conventional fuels. Results indicate that less water-intensive cultivation can be achieved in the Gulf Coast region, where the average water footprints of the three simulated pathways were determined to be 155 m^3 water $tonne^{-1}$ biomass, 371 m^3 water $tonne^{-1}$ algal proteins, and 11 m^3 GJ^{-1} biofuel. The water footprints of algal systems were found to be more favorable when compared to traditional biomass feedstocks

such as soybeans and corn. However, when compared to petroleum-based fuels, results emphasize the need for more water-efficient strategies to reduce the water demands of algal cultivation. This work also incorporates a novel temperature tolerance assessment to identify the geographically specific temperature limits for algal strains in a commercial-scale facility. Results highlight the importance of high temporal and spatial resolution when modeling culture temperature, evaporative loss, and algae growth rate.

ACKNOWLEDGEMENTS

The author would like to acknowledge financial support from the United States Department of Energy (DE-EE0008906 and DE-EE0008902). John McGowan is also acknowledged for performing the experimental work at the Arizona Center for Algae Technology and Innovation that supported this study. The author gratefully acknowledges Jose and Cecilia Quiroz for their unmeasured support. Myself, and all collaborating authors, also thank Danna Quinn for editing the manuscript of the journal submission core to the content of this thesis.

TABLE OF CONTENTS

1. INTRODUCTION

Extreme climate events are increasing in frequency and severity. This, combined with a growing global population, further exacerbates the need for sustainable energy technologies. Algal technologies are expected to play an important role in the effort to phase out petroleum fuels [1]. Algal biomass is considered a potential solution to the multiple demanding challenges of the food, water, and energy nexus. Microalgae can not only provide higher biomass yields per area of cultivation at a faster rate than conventional land crops such as corn and soybean [2]–[4], but can also be integrated with carbon capture technologies [5]–[7], as well as be processed into a variety of co-products such as nutraceuticals, bioplastics, and animal feed [8]–[11]. In contrast to other energy crops, algae can be cultivated on non-arable land, eliminating competition with food crops for high-value farmland [12],[13]. Despite the many advantages of algal biomass, many obstacles must be addressed before the large-scale deployment of sustainable algae farms becomes a reality. Multiple studies have shown that land requirements for sustainable production of algal fuels can be met [14], [15]. Preceding studies have also shown the need for carbon capture instead of the co-location of algae systems to CO_2 sources, and for improvement in the logistics of CO_2 supply and delivery for sustainable scalability of algal biofuels [15]–[17]. In terms of water, there is no general agreement on the water requirements for large-scale production of algae in open-raceway pond (ORP) systems [18], [19] due to limited research in this area [14].

Due to the growing concern over water scarcity and depletion of freshwater sources, it is necessary to provide accurate estimates of water requirements for emerging bioenergy

technologies [20]. Water demand not only has a direct impact on life cycle assessments but also impacts the economics of algae products. Multiple studies have attempted to quantify the water footprint (WF) from microalgae cultivation in ORPs with results ranging from 15.8 to 230 m^3 per tonne of biomass [4], [14], [18], [21]. Most existing studies are limited since they lack high-resolution modeling and often approximate biomass yields with simplified solar conversions for a restricted number of locations [4], [18], [22]. Accurate prediction of biomass productivity requires geographically resolved growth modeling with the ability to capture biological effects at a high temporal resolution [23].

Aside from productivity assumptions, the variability in water footprints is primarily attributed to the range of methodologies and assumptions used to estimate water loss through evaporation from open algae systems [18]. Previous studies often simplify the analysis by using evaporation models that neglect pond temperatures or assume that evaporative behavior in algae ponds follows that of pan evaporation systems [21], [22], [24]. Other studies provide water loss estimates through the coupling of evaporation models to dynamic thermal models with high temporal resolution [14], [25], [26]. This methodology is the most appropriate since it captures important geographical and temporal differences in evaporation rates from algae ponds, but an appropriate selection of the evaporation model and validation data is fundamental to reduce the uncertainty of these assessments [25].

Evaporation from free water surfaces is a function of the water surface temperature and meteorological conditions such as relative humidity, vapor pressure, wind speed, and ambient temperature. Methods for modeling evaporation rates from free water surfaces range in complexity and accuracy [27]. The most simple and inaccurate is the pan evaporation method, but more physically sound models that capture meteorological-based effects have been used in

studies focusing on the water demand of algal ponds [4], [14], [18], [25]. These models often rely on empirical equations correlating wind speed to evaporation and are designed to estimate evaporation rates from lakes or cooling ponds [28]–[30]. Béchet et al. [25] reviewed and tested several evaporation models against experimental data measured in a pilot-scale pond and concluded that purely empirical evaporation models fail to accurately predict evaporation rates from algal systems since they were originally validated for water bodies with different spectral characteristics (algae cultures are more opaque), depths, and surface area [25], [29]. Béchet et al. [25] recommended a flat-plate model derived from theoretical concepts based on its accuracy and versatility to capture system-scale effects [25]. More importantly, the need to account for both mass transfer modes (natural and forced convection) is crucial when modeling systems with a larger surface area, such as commercial algae ponds, as the evaporation rate is inversely related to the characteristic length of the system [25], [29], [31].

Equally critical is the need to validate thermal models with experimental data relevant to the system properties and scale. Studies in the literature often use observations from elevated experimental algae raceways to validate thermal models, which may provide inaccuracies when extrapolating results for commercial algae ponds [26], [32]. Khawam et al. [33] demonstrated that the temperature profiles from elevated raceways differ from those in commercial ponds. These variances are fundamentally linked to evaporation effects amplified by the paddlewheel. The additional turbulence and increase of pond surface area caused by the paddlewheel have a direct impact on the evaporation rates of experimental ponds. Therefore, to reduce the uncertainty in the computation of evaporation rates from commercial ponds, evaporation models must be validated at a pond scale where paddlewheel effects are minimal. Wigmosta et al. [14] validated an empirical evaporation model using corrected pan evaporation measurements. The

water used in pan evaporation has different spectral properties than algae cultures and wind effects are not completely captured due to the small surface area of evaporation pans [18], [25], [27]. When compared to annual net lake evaporation rates, White and Ryan [34] measured higher evaporation rates from a commercial algae farm located in New Mexico. This is likely associated with the contrasting depths between shallow microalgae ponds and deeper lakes.

Clearly, there exists a need for a robust temporal and geographical assessment of the water requirements for large-scale production of algal biomass. Although Wigmosta et al. [14] provided a novel and thorough outlook on the land and water requirements for large-scale algae farms, the assumptions used result in high uncertainty when estimating evaporation rates at larger scales. This study provides estimates for the blue WF of microalgae cultivation computed with a dynamic thermal and biological model developed and validated to predict evaporation losses, temperature profiles, and areal productivity of large-scale systems. This foundation is integrated with life cycle methodology to determine the WF of three different algal-based products. Results include water demands and temperatures for two different farm scales (400 and 4000 hectares) for 198 locations across the US over 21 years, as well as the uncertainties in predicting water demand and pond temperatures using typical meteorological year (TMY) data [35] and actual weather data sets. The discussion focuses on the co-dependence of evaporation, temperature, and growth in algae systems, highlights the importance of accurate co-modeling of these parameters, and includes a comparison of WF of conventional energy crops cultivated for fuels and proteins. Lastly, the work is used to estimate temperature tolerances with a geospatial resolution to support strategic large-scale cultivation of algal strains.

2. MATERIALS AND METHODS

This study is built upon accurate computations of water demands and biomass production at high temporal and spatial resolutions. Evaporation losses were determined using an energy balance approach through dynamic thermal modeling, while biomass productivity yields were estimated using a coupled biological growth model [26]. Although both models function as an integrated unit, validation of the thermal and biological model was performed independently using experimental observations for pond temperature, depth, and algal concentration. When coupled with historical meteorological data, model capabilities allow for a geographical and temporally resolved assessment of the WF of algal systems. The following sections provide detailed descriptions of the water footprint methodology, thermal model, biological model, validation data, and the simulation approach used in this work.

2.1 Water footprint methodology

The goal of this study was to compute the water footprint of large-scale algae cultivation systems and to compare them to those of traditional energy crops. As defined by Gerbens-Leenes et al., the blue WF of a product measures the amount of water consumed from blue water resources such as groundwater and rivers. The green WF quantifies the amount of water consumed from precipitation, while the gray WF component refers to the amount of freshwater needed for waste streams to meet water quality standards based on the concentration of pollutants [36]. In the case of algae cultivation, the blue component includes the water needed to replace evaporation losses and is expressed in terms of biomass productivity or energy content [19], [36]. It is important to note that this analysis only considers the WF associated with the

algae cultivation process in ORPs and excludes water requirements from downstream conversion processes. Indirect water consumption from process consumables such as nutrients and electricity were assumed to be supplied from a non-local water source and were therefore not included in the water balance. Using these assumptions, the local on-site water footprint was calculated and reported in terms of cubic meters of water per functional unit. The water intensity of three different pathways producing distinct algae products was calculated: algal biomass, proteins, and biofuels. Functional units for algal biomass, algal proteins, and biofuels were set to a tonne of ash-free dry weight (AFDW) biomass, a tonne of algal proteins, and GJ of biodiesel, respectively. Green and gray WF components were not considered in order to simplify the analysis.

2.2 Thermal model

Thermal modeling is the foundation of this analysis, thus, a high-fidelity thermal model capable of providing accurate simulations of temperature and evaporation rates is essential to reduce error propagation in subsequent computations. The thermal model used in this study is a modification of the model developed by Greene et al. [26]. The model performs a transient energy balance for an isothermally spatial system to calculate time-resolved thermal outputs based on the algae culture's thermal properties and various heat fluxes driving the thermal behavior of the pond [26]:

$$\rho c_p V \frac{dT_p}{dt} = \sum Q_n \quad (1)$$

where ρ denotes the culture density [kg m^{-3}], c_p is the specific heat of the culture [J kg^{-1} K^{-1}], V is the pond's volume [m^3], T_p is the temperature of the culture [K], t is the independent time coordinate [s], and $\sum Q_n$ is the sum of the heat fluxes [W]. Heat fluxes include direct and diffuse solar radiation, water inflow, pond radiation, atmospheric radiation, ground conduction,

convection, and evaporation. The governing equation was integrated in time using a fourth-order Runge-Kutta method with a fixed time-step of one hour [25].

Primary model inputs include parameters describing the geometry of the pond such as the length, width, and operating depth, and meteorological conditions: global horizontal irradiance (GHI), ambient temperature, relative humidity, and wind speed. To predict accurate evaporation rates and pond temperatures, the following heat transfer models were modified from Greene et al. [26]: atmospheric radiation, ground conduction, convection, and evaporation. The methods selected to model these heat transfer mechanisms are explained in detail in the following sections. Heat transfer models that were not modified are included in the Appendix.

2.1.1 Atmospheric radiation

The atmospheric radiation heat flux was found to be a highly sensitive forcing term dependent on the ambient temperature (T_{amb}) and sky emissivity (ε_{sky}). The method to calculate the radiation emitted by the atmosphere to the pond is defined by the Stefan-Boltzmann law:

$$Q_{atmo} = \varepsilon_{sky} \cdot \sigma \cdot A_s \cdot T_{amb}^4 \quad (2)$$

where σ is the Stefan-Boltzmann constant, A_s represents the surface temperature, and T_{amb} is the ambient air temperature [K] [37]. The sky emissivity was calculated using the Brunt equation, previously used for algae pond models by Khawam et al. [33]:

$$\varepsilon_{sky} = a + b \cdot \sqrt{p_a} \quad (3)$$

where a and b are empirical coefficients set to 0.6 and 0.031 [mm $Hg^{-0.5}$], and p_a is the saturated vapor pressure at the ambient temperature in mm Hg [38].

2.1.2 Ground conduction

The conductive heat transfer between the pond and ground plays an important role in lowering pond temperatures during periods of intense solar radiation. Ground conduction is a function of the thermal properties of the soil beneath the pond which include thermal conductivity (k_g), and the thermal diffusivity (α_g). The heat transfer interactions between the pond and ground are calculated using the solution for the heat diffusion equation. This solution assumes a constant pond temperature during the duration of the time-step and takes the form:

$$Q_{ground} = \frac{k_g \cdot A_s \cdot (T_P - T_g)}{\sqrt{\pi \cdot \alpha_g . h}} \quad (4)$$

where T_g is the ground temperature assumed to equal the annual average ambient temperature or the average for the period of the analysis [37], [39], [40], and h is the time-step of the analysis [37], [40]. The thermal conductivity was empirically calibrated to 1.7 [W m^{-1} K^{-1}] and the thermal diffusivity was set to 7.9×10^{-6} [m^2 s^{-1}], in accordance with values in the literature [40].

2.1.3 Convection

Convective effects at the pond surface deserve special attention, especially when modeling ponds with large surface areas. This study uses a semi-empirical flat plate model to calculate heat transfer via convection. Different from other studies, this model accounts for convective effects from both natural and forced convection, which are calculated using correlations that relate the size of the system to the wind speed (forced convection) and density gradient (natural convection). To simplify model operations, the effects of wind direction were not considered by defining the characteristic length of the system to be the ratio of surface area to perimeter of the pond. The forced convection model is taken directly from Greene et al. [26],

while natural convection effects are calculated using the following Nusselt number correlations for the laminar and turbulent regime, respectively:

$$Nu_L = x \cdot Ra_L^{1/4} \ for \ (10^4 \ \leq Ra_L \leq 10^7, \text{Pr} \geq 0.7) \quad (5)$$

$$Nu_L = y \cdot Ra_L^{1/3} \ for \ (10^4 \ \leq Ra_L \leq 10^{11}, \text{Pr} \geq 0.7) \quad (6)$$

where x and y are empirical coefficients set to 0.54 and 0.15, and Ra_L is the dimensionless Rayleigh number [37]. In the case where mixed natural and forced convection effects are present, the following correlation was used:

$$Nu_L = \left(Nu_{L,f}^n + Nu_{L,n}^n\right)^{1/n} \quad (7)$$

where $Nu_{L,f}$ and $Nu_{L,n}$ are the Nusselt numbers obtained from the forced and natural convection correlations, and n is an empirical coefficient set to 3 [37]. Forced convection correlations and convective heat flux equations are further described in the Appendix.

2.1.4 Evaporation

As previously mentioned, the selection of an appropriate evaporation model is paramount to produce robust water demand estimates. The mass transfer correlations used to model evaporation are analogous to the convection correlations presented in the previous section. Similarly, both mass transfer from forced and natural convection were considered. The main advantage of this evaporation approach over others in the literature is the use of nondimensional parameters which provide a method to scale up results from pilot-scale ponds to commercial ponds. Additionally, by separating the forced and natural convection components, the appropriate accounting of both transport phenomena is ensured. Methods to model evaporation from forced convection effects followed the ones used in Greene et al. [26]:

$$Sh_L = c \cdot (Re_L)^{0.5} (Sch_L)^{\frac{1}{3}} \qquad \text{for } Re_L < (3 \times 10^5) \ (8)$$

$$Sh_L = d \cdot (Re_L)^{0.8}(Sch_L)^{\frac{1}{3}} \qquad \text{for } Re_L > (5 \times 10^5) \quad (9)$$

The empirical coefficients c and d were calibrated to 0.65 and 0.045, respectively. The natural convection correlations for mass transfer have the form of Eqs. (5,6), previously defined by Lloyd et al [41]:

$$Sh_L = x \cdot Ra_L^{\frac{1}{4}} \; for \; (2.2 \times 10^4 \; \leq Ra_L \leq 8 \times 10^6) \qquad (10)$$

$$Sh_L = y \cdot Ra_L^{\frac{1}{3}} \; for \; (Ra_L > 8 \times 10^6) \qquad (11)$$

where Sh_L is the dimensionless Sherwood number[41]. The approach for mixed mass transfer follows that of Eq. (7), substituting the Nusselt number for its mass transfer counterpart, the Sherwood number. Once the Sherwood number is defined, the evaporation rate m_e [kg m^{-2} s^{-1}] can be determined:

$$m_e = \frac{Sh_L \cdot D_{wa}}{L_c} \cdot \left[\frac{p_w}{T_p} - \frac{RH \cdot p_a}{T_{amb}}\right] \cdot \frac{M_w}{R} \qquad (12)$$

where $D_{w,a} = 2.4 \times 10^5$ [m^2 s^{-1}] denotes the mass diffusion coefficient of water vapor in the air, L_c is the characteristic length [m], RH is the relative humidity of the ambient air, $R = 8.314$ [Pa m^3 mol^{-1} K^{-1}] is the ideal gas constant, and p_a and p_w [Pa] are saturated vapor pressures at T_{amb} and T_p, respectively [18], [26], [42]. The heat transfer is then calculated using the following equation:

$$Q_{evap} = -m_e \cdot L_w \cdot A_s \quad (13)$$

where $L_w = 2.45 \times 10^6$ [J kg^{-1}] is the latent heat of the water.

2.3 Biological model

To determine microalgal biomass yields, this study adopted the biological modeling methodology developed by Greene et al. [26]. This model calculates algae growth based on the

primary physical processes affecting growth: culture temperature, respiration losses, and light availability impacted by culture concentration and incoming solar radiation [26]. The model correlates a carbon fixation rate to multiple efficiency factors which serve to account for conditions deviating from optimal. The rate of algal concentration is calculated using the following equation:

$$\frac{dC_x}{dt} = \frac{C_1 \cdot 0.458 \cdot GHI \cdot \varphi_L(t) \cdot \varphi_T(t) \cdot \emptyset_{photon} \cdot A}{V} + \frac{D(t)}{V} \qquad (14)$$

where $C_1 \cdot 0.458 \cdot GHI$ represents the conversion from GHI to photosynthetically active radiation (PAR) in the 400-700 nm range, $\emptyset_{photon}$ is the photon efficiency in terms of grams of biomass per mol photon, A is the surface area of the pond, V is the volume of the pond, $D(t)$ is the decay rate quantifying biomass losses from dark respiration, φ_L and φ_T are the light and temperature efficiencies, respectively [26].

The calculation of algal growth begins by defining a carbon to photon conversion factor, which has a range of 1.2 to 1.5 [g biomass per mol photon] according to Greene et al. [26]. The model proceeds to quantify temperature effects on carbon fixation through a cardinal temperature model. This temperature model requires the input of four parameters describing the temperature response of the organism: minimum and maximum temperatures tolerated by the microalgae strain, the optimal temperature for growth, and the pond temperature (provided by the thermal model). The light efficiency component considers photoinhibition and concentration effects of the algae culture to provide a light efficiency ranging from zero to unity. Concentration effects are quantified using a depth-integrated Beer-Lambert's law and the assumption that the culture is well-mixed [26]. To calculate light response effects, two specific strain parameters must be defined: the optical density coefficient (defined as the slope of the curve comparing biomass concentration [g m^{-3}] and the optical density [OD_{750}]) and the saturation light intensity. The final

foundational input of the growth model is the percent of biomass lost during dark respiration, used along the temperature efficiency factor to compute the decay rate [26]. After a complete species characterization is achieved, the model proceeds to calculate the time-resolved culture concentration. Further details are presented in Greene et al. [26].

2.4 Thermal and biological model validation

Experimental data was leveraged to validate both the thermal and biological models. The thermal model was validated with data from the literature. Temperature and pond depth observations measured by Béchet et al. [25] in their comparison study were used to assess the model's accuracy. To the authors' knowledge, the data set used by Béchet et al. [25] is the most detailed collection of parallel temperature and pond depth measurements from a pilot-scale ORP system in the literature. Similarly, the growth model was validated with algal concentration data from the trials performed at the Arizona Center Algae Technology and Innovation (AzCATI). The growth model validation data includes on-site measurements of PAR, pond temperature, and algal concentration for an elevated experimental ORP. Both tools were verified and validated separately to provide an unbiased assessment of model quality.

Thermal validation data included all foundational inputs required to compute simultaneous pond temperatures and evaporation rates at an hourly resolution. As detailed by Béchet et al. [25], the pond used for this analysis was refilled regularly during the first half of the study and left to evaporate during the latter trials. The data set was reduced by eliminating periods where either evaporation or temperature measurements seem to vary (likely due to instrumentation issues, pond harvesting, or rainfall events) resulting in a total validation period of 314 days. Model inputs with the highest uncertainty were used to calibrate the model. Among these parameters are the soil properties, absorptivity and emissivity of the culture, and the

empirical coefficients of the convection and evaporation correlations. These parameters were bounded by retrieving minimum and maximum values from the literature. The final calibrated values were chosen by simultaneously minimizing the evaporation and temperature error through the entire validation period using a multiobjective optimization algorithm in MATLAB®. Rainfall events were considered of low impact and were not included in the thermal balance calculations.

The temperature error was calculated by comparing the hourly model to the hourly measured pond temperatures. The evaporation error is reported using two different metrics. The error is first reported as the relative mean percentage error obtained from comparing the hourly model to the measured pond depth. In addition, as a means to compare to previous studies, the evaporation error was also calculated by comparing the total modeled evaporated depth during the validation period to the total measured evaporated depth, following the methods in Béchet et al. [25].

Similarly, the growth model was validated with experimental data collected in the summer of 2019 from growth experiments of *Acutodesmus obliquus* (UTEX 393) grown at AzCATI in Mesa, AZ (33.41° N, 111.83° W). Three elevated experimental ponds, each with a surface area of 4.2 m^2 and a volume of 820 L, were operated semi-continuously at a depth of 20 cm. The culture was grown in BG-11 media with ammonium bicarbonate as the N-source and a 16:1 N:P ratio with 5 ppt salinity. Algal concentration was measured in triplicates during the morning and afternoon. Simultaneous measurements of pond temperature and PAR were collected on-site. The selected data were collected from June 2019 to August 2019 resulting in a total of 24 harvests, from which three were discarded based on a statistical analysis of the grams to PAR ratio for that period. UTEX 393 is characterized as being a summer tolerant strain with

high saturation light intensity and temperature tolerances. Experimental pond temperature and PAR were input into the growth model along with six model inputs characterizing the strain, listed in the Appendix. The model was calibrated with half of the data set and validated with the remaining harvests. The error was calculated by comparing the measured algal concentration to the modeled output.

2.4 Simulation framework

The simulation approach used in this study integrates the validated thermal and growth model with historical meteorological data and a harvesting scheme to predict pond temperatures, evaporation rates, and biomass yields. Thermal simulations were done for two different algae farm sizes with weather data from two different sources, resulting in a total of four scenarios. Results for each of the selected locations were generated in MATLAB® and spatially interpolated in R using kriging interpolation to cover the contiguous United States (CONUS) and Hawaii. Simulation outputs include heat maps illustrating regional variances in water demand and water footprints for microalgal biomass, proteins, and biofuels. Also, the work includes a novel analysis of geographical and seasonal temperature sensitivity which might inform strain optimization studies and provide insights on productivity maximization methods for open algae cultivation systems.

2.4.1 Meteorological data

Historical weather data comprising of hourly measurements of solar radiation, wind speed, relative humidity, and air temperature were retrieved from the National Solar Radiation Data Base (NSRDB) [43] and the typical meteorological year (TMY3) files from the National Renewable Energy Laboratory (NREL) [35]. The NSRDB files contain data from 1998 to 2018 from 198 locations across the U.S. Each of the locations was simulated by resetting the model at

the start of each year. The TMY3 files are comprised of hourly data from 903 locations in the US. Results generated from the two data sets were compared to assess if the analysis could be simplified by using TMY3 data without a significant loss in accuracy.

2.4.2 Facility design and operation

Results for two different farm sizes were generated to gain a better understanding of the implications of facility size on water demands. The baseline scenario models an algae farm with an area of 400 hectares, based on techno-economic assessment (TEA) and resource assessment (RA) models in literature [14], [15], [44]–[47]. The second scenario considers a 4000-ha farm sized according to projected biomass requirements by downstream conversion processes [47]–[49]. To simulate real-time facility operations, the growth model was coupled with a dynamic harvesting scheme. Ponds were assumed to be operated semi-continuously with an initial concentration of 0.1 g L^{-1}. Harvesting was assumed to occur at the first of either achieving 0.45 g L^{-1} or 3 days from system inoculation.

2.4.3 Biomass conversion

A high-level conversion process from algal biomass to proteins and fuels was modeled to establish a global and objective comparison to other energy crops. The protein content of the modeled strain was assumed to be 41.7 % [50]. Conversion to fuels was done via hydrothermal liquefaction (HTL), assuming a biocrude yield of 50 wt. % of AFDW (0.5 kg biocrude per kg AFDW) and a biocrude to diesel and naphtha conversion of 63 % and 11 % by weight, respectively [17], [49], [51]. Energy content from algal biodiesel was calculated assuming a high heating value of 35 MJ kg^{-1} [52] and an oil density of 0.92 kg L^{-1} [14]. The computed water footprints of algae systems were then compared to those of primary and secondary bioenergy

crops such as sugar beet, alfalfa, sugar cane, maize, barley, sorghum, and soybean [20], [53]–[56]. Blue WF for conventional feedstocks is provided in the Supplementary Information.

2.4.4 Temperature tolerance

Pond temperatures have been shown to have an important impact on the growth rates, reliability, composition, and overall performance of algae species grown in ORPs [33], [57]–[60]. Therefore, a comprehensive understanding of the temperature limits of commercial ORPs is not only critical for the appropriate siting of algae cultivation facilities but also to support strain selection decisions. This study provides temperature profiles of commercial ORPs computed with historical weather data and a validated thermal model designed to predict temperatures in commercial ORPs. The temperature profiles for the 400-ha baseline scenario were processed to determine the maximum temperatures for three different time intervals: a one-hour, two-hour, and three-hour culture exposure. Moreover, the simulated pond temperatures for five distinct locations were examined to identify seasonal and geographical trends based on descriptive statistics. Results from the temperature tolerance assessment include dynamic maps illustrating maximum temperatures reached in commercial algae facilities and a geographical and temporal comparison of pond temperatures of commercial-scale facilities. Finally, the interactive effects of temperature and exposure time to avoid temperature-related culture crashes were investigated.

3. RESULTS AND DISCUSSION

The results of this study are presented in three different sections, 1) results obtained from the validation of the thermal model including error in the predicted temperature and evaporation rates, 2) results and errors associated with the validation of the biological model, and 3) results obtained from the simulation process including national productivity yields, water footprints, and temperature tolerance analysis.

3.1 Thermal model validation

The thermal model validation process quantifies the model's ability to simultaneously predict pond temperatures and evaporation rates accurately. The error was quantified by comparing a total of 7,525 data points. Plot regressions illustrating model accuracy are presented in Figure 1. The temperature accuracy shows an average error of -0.96 ± 2.72 °C, consistent with values reported in the literature for previous validation efforts [26], [42], [61]. The highest average temperature errors were seen in the winter and spring season, where lower temperatures were predicted. The lower modeled temperatures during these months are an effect of the overprediction of evaporative cooling. Furthermore, wind speed measurements were the highest during the spring and winter months, as seen in Fig. S1; this likely indicates that temperature errors are directly correlated to evaporative effects.

The average annual evaporation error was calculated to be 1.46 ± 5.92 %. In terms of the total evaporated depth, the model demonstrated an overall under-prediction of 20.2 %, which is within the range reported by Béchet et al. [25]. The winter and summer seasons presented the highest evaporation errors of 5.69 ± 3.71 % and -3.24 ± 4.7 %, respectively. Wind speed data

was found to be the primary driver of evaporation error. The error seen during the winter months is linked to high wind speeds and lower relative humidity conditions during these months. Similarly, the summer error was also found to be highly correlated to wind speed measurements. Pond temperatures increased over periods of low wind speeds, causing the model to underestimate evaporative cooling effects (see Fig. A4). These thermal validation results highlight the importance of accurate wind speed measurements to reduce the uncertainty in predictions of evaporation rates. The data from the seasonal analysis of the validation effort and time-series for both temperatures and pond depths are shown in the Appendix.

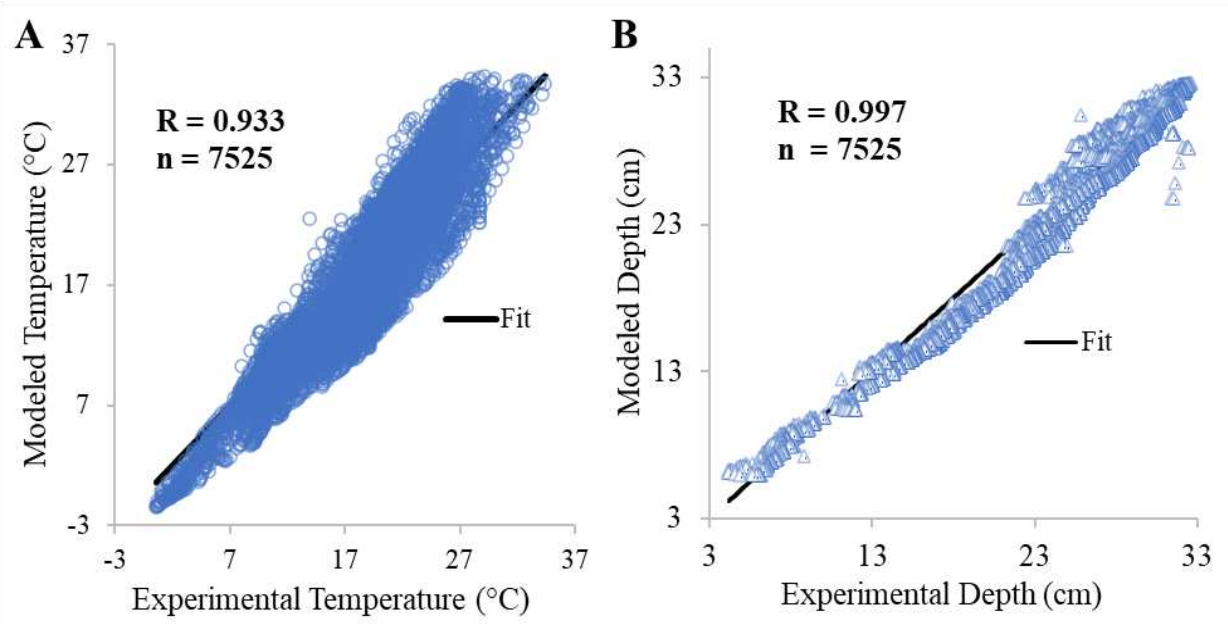

Figure 1. Modeled versus experimental pond (A) temperature and (B) depth. Average annual temperature error: -0.96 ± 2.72 °C. Average annual evaporation error: 1.46 ± *5.92 %. Although a high R-value was obtained from the evaporation model, a 20.2 % error was calculated when comparing the total measured and modeled evaporated depths during the validation period.*

3.2 Biological model validation

The growth model validation in this study quantifies the predictive error and evaluates the model's performance in simulating growth rates of UTEX 393. Experimental and modeled biomass concentration (AFDW) for the validation data set is illustrated in Fig. 2. The model provided accurate predictions of concentration over the simulated period with an average relative error of -4.59 ± 8.13 %. The error from the biological model is within the range of previously reported values for this specific strain [62]. When comparing the areal productivity for the summer 2019 growth campaign, the model calculated areal productivity of 27.7 g per m^2-day, which translates to an underestimating error of 1.82 %.

In addition, this predictive error was found to be highly sensitive to the strain's saturation light intensity. UTEX 393 is considered an all-season strain with peak performance occurring in the summer months. The biological model was not coupled with the thermal model for validation given that the temperature profiles of the systems used for thermal and biological validation are different due to system differences (the experimental system is an elevated small-scale pond). Growth data was obtained from experimental ponds where the paddlewheel enhances evaporative cooling. Determining temperature with the current thermal model would have introduced unnecessary error since the model was not built to capture paddlewheel effects.

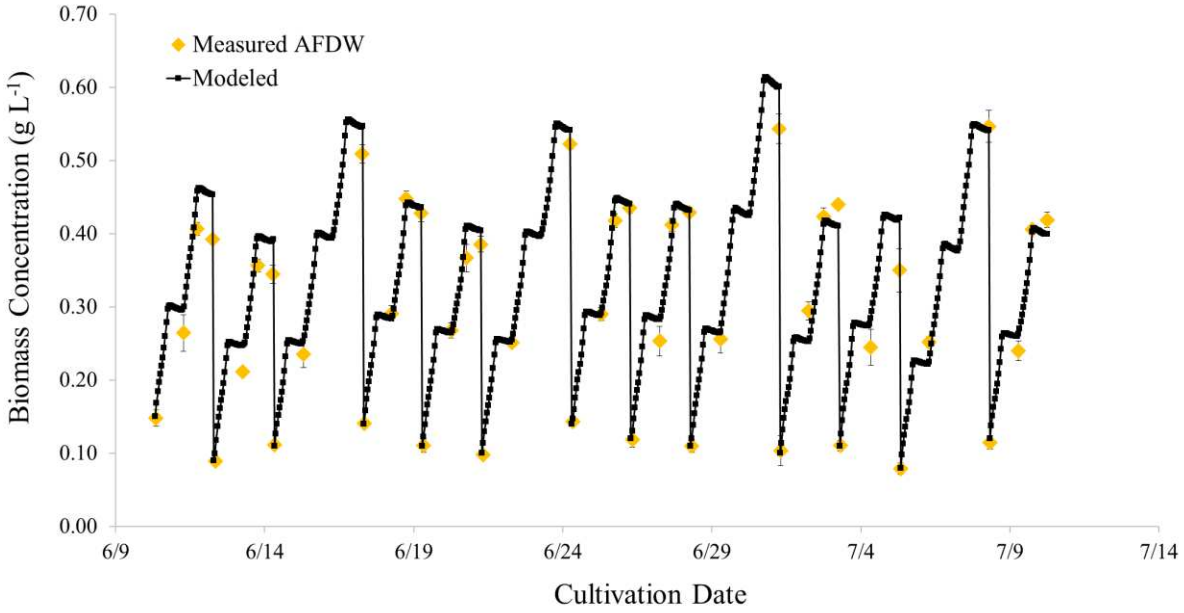

Figure 2. Biological model validation for the summer 2019 runs of Acutodesmus obliquus UTEX 393. A total of 12 harvests were simulated, the initial biomass concentration for each of the semi-continuous runs was set to the respective concentration in each run. Error bars on the measured data represent the standard deviation of the algal concentration of 3 different ponds. The biological model showed an average error of -4.59 ± 8.13 %.

3.3 Model extrapolation

The following section presents the results generated from the simulations conducted with the coupled thermal-biological model. The results from the model extrapolation effort are divided into four sections: (*i*) water demand (*ii*) microalgae productivity, (*iii*) water footprints, and (*iv*) results from the temperature tolerance analysis.

3.3.1 National water demand

The water demand for the different combinations of weather data sets and facility scales were determined and leveraged to identify regions with the highest water demands for algae cultivation. Results for the baseline scenario of a 400-ha facility generated with weather data from the NSRDB are illustrated in the form of a dynamic map covering the CONUS and Hawaii.

As depicted in Fig. 3, marked regional differences exist when it comes to evaporation losses. As expected, water demands are the highest in the desert southwest region, where high light intensity and dry conditions predominate. Annual water demands reached a maximum of 16.8 ML-ha^{-1} in this area. The Gulf Coast region and Hawaii, where more humid conditions are present, land on the middle to lower range of the spectrum. The lowest evaporation losses are seen at the northern latitudes where lower temperatures and light intensity predominate. A national annual mean of 7.38 ML-ha^{-1} was determined.

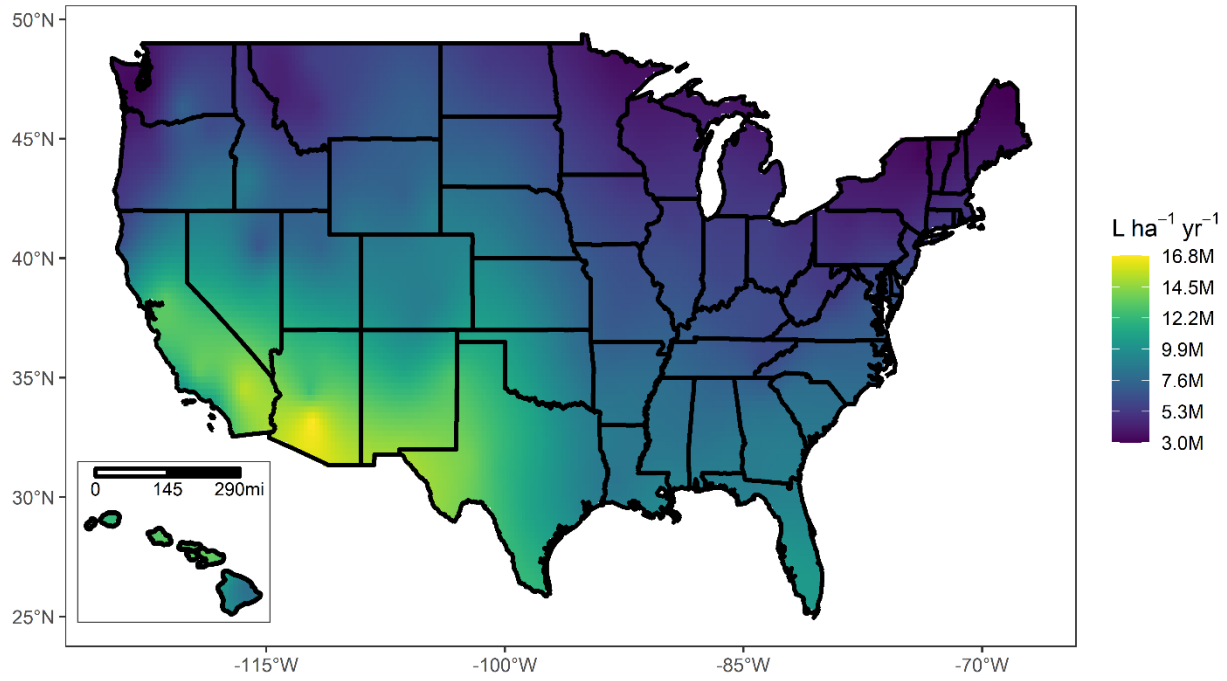

Figure 3. Mean annual water demand (L ha^{-1} yr^{-1}) for a 400-ha cultivation facility calculated with weather data from the NSRDB. Results represent the annual mean of 21 years (1998-2018). A national average of 7.4 ± 2.9 ML ha^{-1}yr^{-1} was calculated.

Compared to the literature, the water losses calculated in this study follow the same geographical trends provided by Wigmosta et al. [14] but with key differences in the upper and lower limits. Wigmosta et al. [14] estimated water demands in the Gulf Coast region averaging

1.53 ML-ha^{-1}, significantly lower than the average of 9.5 ML-ha^{-1} calculated in this study. When comparing the desert southwest region, the annual average water demand computed in this study is 12.3 ML-ha^{-1} compared to 10.2 ML-ha^{-1} estimated by Wigmosta et al. [14], representing a 20% increase. The variability in results is likely due to the contrasting approaches used in the model validation, particularly within the evaporation models and data used for validation.

Additionally, historical pan evaporation data curated by Dewes et al. [63] was used to approximate the differences in evaporation rates from commercial microalgae ponds and pan evaporation measurements. Water demand results were found to be significantly lower than pan evaporation measurements with an average absolute difference of 59 %. For corrected pan evaporation or lake evaporation, this average reduces to 45 %. These variations decreased at locations with lower wind speeds, implying that pan evaporation methods fail to capture wind effects present at commercial-scale algae ponds. The data demonstrates that the differences in depth and surface area of these systems make pan evaporation data inadequate to model evaporation from commercial algae ponds.

The additional scenario modeled with weather data from the NSRDB provided further evidence of the interconnection between wind speed, surface area, and the magnitude of water demands. The results indicate lower evaporation rates as the system size increases. When comparing water demands from the 4000-ha facility scenario to the previously simulated 400-ha sized facility, the calculated annual water demand decreased by an average of 4 %. This reduction in evaporation is evidently an effect of the size of the system. As the area of the facility increases, the effects of wind speed are less relevant since evaporation is primarily driven either by a combination of forced and natural convection (mixed convection) or purely by buoyancy effects. Changes in water demand were the lowest in areas with low wind speeds as shown in

Fig. A11. These results show that water loss at the 400-ha scale is representative of larger-scale systems.

Evaporation results were also compared to simulations with TMY3 data. Results generated with the TMY3 data set follow the same regional trends, but with a wider range for both facility sizes. The difference in water demands between the 400-ha and 4000-ha for the TMY scenario is more pronounced than those computed with weather files from the NSRDB. Results generated with TMY3 data show a 14 % reduction in the water demands of a 4000-ha compared to a 400-ha facility, which is more than three times higher than what was found with weather data from the NSRDB (4%). This difference is higher than the results calculated with the NSRDB files due to the low accuracy of wind speed measurements in TMY3 files. TMY3 data was originally developed to mimic typical conditions for solar radiation measurements and assigns lower weights to wind speeds, which might contribute to propagating error in the evaporation calculations. This is confirmed by observing the results from the weather data comparison. The average absolute difference in water demands between the results generated with TMY3 and NSRDB files for a 400-ha facility was calculated to be 16 % (Fig. A15). For a system size of 4000-ha, the average difference in water demands decreases to 8 % (Fig. A15) attributed to the small influence of wind speeds at this scale. These results indicate that accurate evaporation modeling requires robust wind speed data.

3.3.2 Geographically resolved biomass productivity

Areal productivity yields from semi-continuous cultures of UTEX 393 were computed to provide a national landscape of the current productivity potential. The computed annual biomass productivity values of the simulated locations were averaged and surface interpolated to define the optimal areas for algae cultivation based on the current state of technology. The outputs are

illustrated in the dynamic map shown in Fig. 4. The maximum biomass yields are located in Hawaii and Key West, FL reaching annual yields above 23 g m^{-2} day^{-1}. In the case of the desert south-west region, outputs show that productivities above 15.5 g m^{-2} day^{-1} can be attained with moderate seasonal variability. Seasonal variability at middle latitudes is more pronounced. For example, facilities in northern Nevada presented summer biomass yields above 14.2 g m^{-2} day^{-1}, but biomass productivity during the fall and winter months was substantially lower due to temperature effects resulting in an annual average productivity of 7.5 g m^{-2} day^{-1}. Results suggest that reducing seasonal variabilities in middle and northern latitudes would require temperature regulation strategies or strains with a wider temperature tolerance.

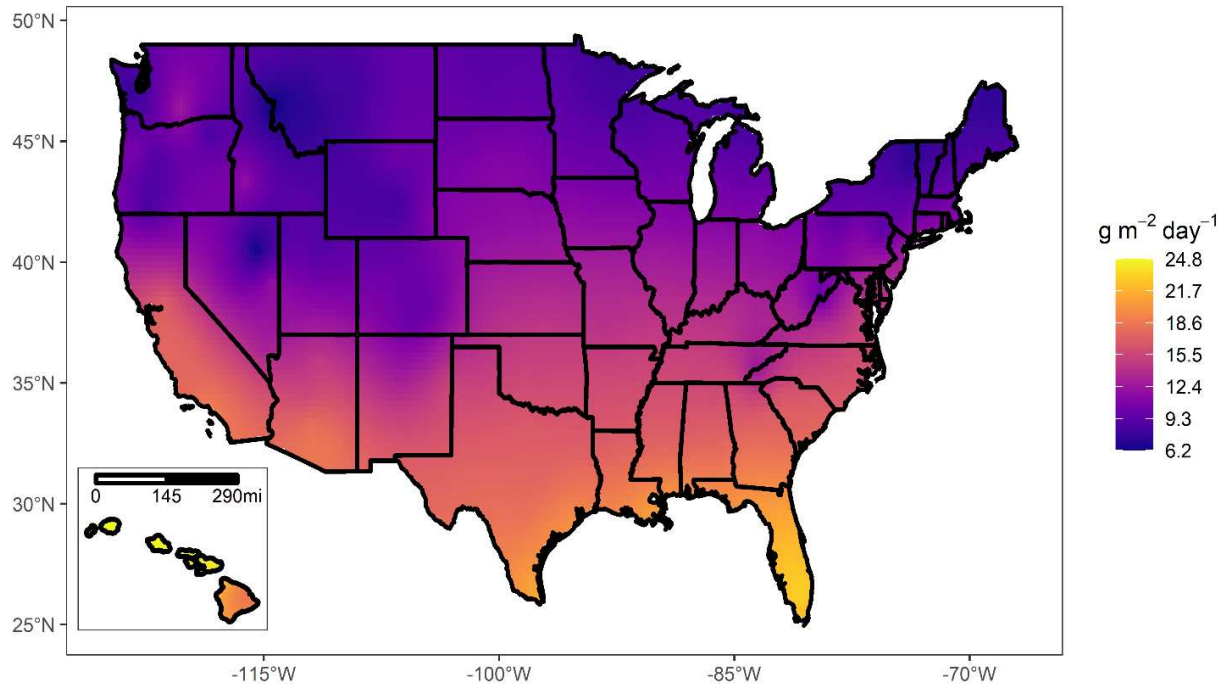

Figure 4. Mean annual biomass productivity (g m^{-2} day^{-1}) yields of Acutodesmus obliquus (UTEX 393) for the conterminous US and Hawaii. Results represent the annual mean of 21 simulated years (1998-2018) using the computed temperature profiles of a 400-ha facility. A national annual mean of 12.1 g m^{-2} day^{-1} was calculated.

The results represent an optimistic scenario of biomass production based on model extrapolation from elevated raceways operated at Mesa, AZ. The modeled annual average productivity of 18.1 g m^{-2} day^{-1}, at this location, was calculated to be 14 % higher than the annual average of 15.9 g m^{-2} day^{-1} obtained from cultivation experiments [50]. These productivity differences are likely associated with the differences in temperature profiles of elevated raceways to commercial ORPs, more details are provided in the following sections. The predicted open pond productivities provide a general outlook of the current biomass production potential at a national scale and illustrate the gap between the current state of technology and the target of 25 g m^{-2} day^{-1}, typically modeled in sustainability assessments [16], [64], [65].

3.3.3 Water footprint assessment

After computing water demands and biomass yields, the spatial variation of the WF of conventional algae systems was assessed. The WF corresponding to biomass, algal proteins, and algal fuels are shown in Fig. 6. The locations with the largest local WF are those with either low productivity and high water demands or areas with high water demands and lower biomass yields. As depicted in Fig. 6, these conditions are prevalent in the Western US, specifically in the middle latitudes where both dry conditions and low productivities intersect. The national average of the blue water footprints of algal biomass, proteins, and fuels was calculated to be 157 m^3 water $tonne^{-1}$ biomass (AFDW), 376 m^3 water $tonne^{-1}$ algal proteins, and 11.2 m^3 GJ^{-1} biofuel for these three different pathways.

The calculated WF of algal systems was compared to those of traditional biomass feedstocks. When comparing the WF per tonne of biomass, microalgae cultivation was found to be less water-intensive than most conventional crops except for drought-tolerant crops such as alfalfa and sugar beet. When compared to maize and soybeans, the results suggest that the

cultivation of algal biomass requires 58 % less water than maize and 89 % less than soybean cultivation. In terms of proteins, the WF is constrained by the protein content of the feedstock. Microalgae contain the highest protein content among the reviewed crops followed by soybean and alfalfa, which carry a WF of 3,741 and 689 per tonne of proteins, respectively. Results emphasize the potential of algal proteins over conventional systems; compared to algal proteins, alfalfa consumes 83 % more water while soybean proteins require approximately ten times more water.

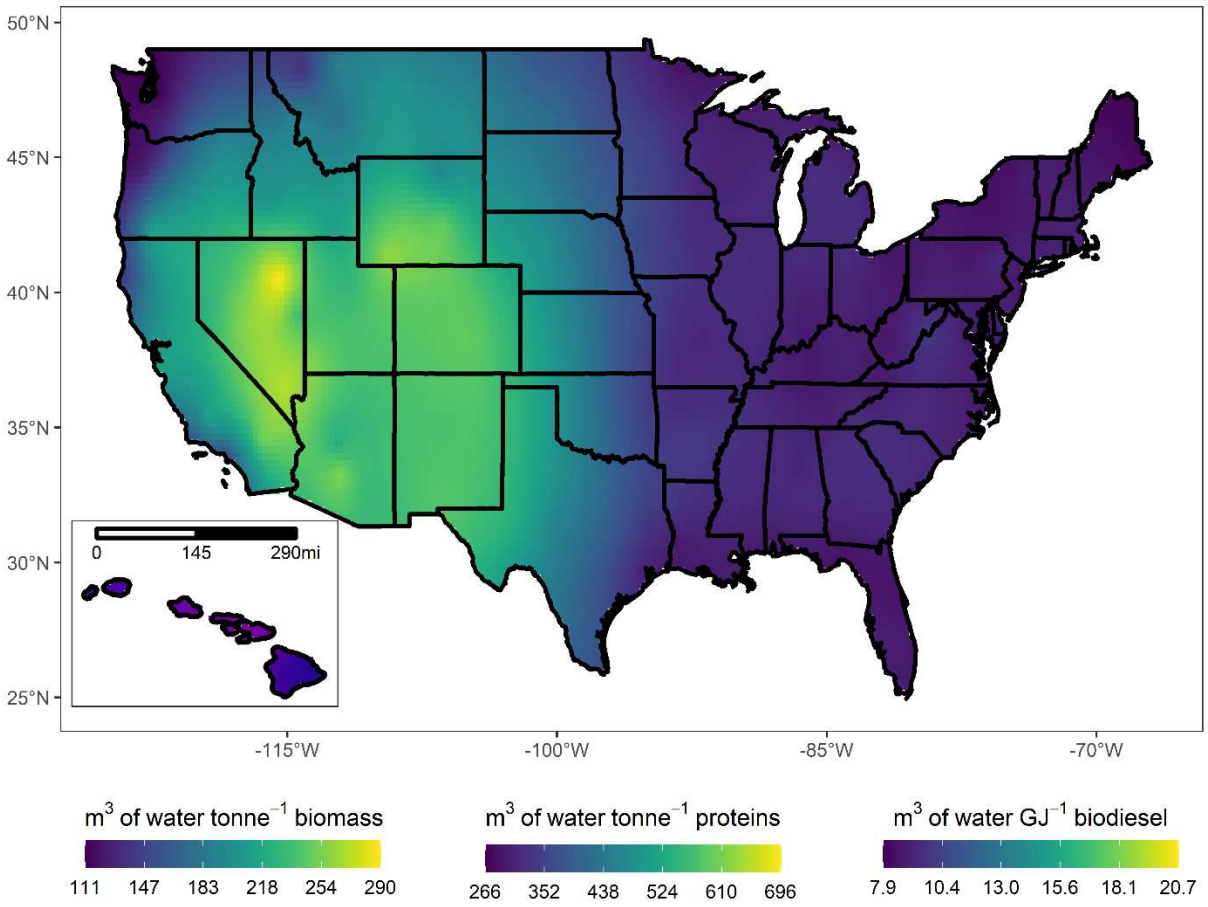

Figure 5. Mean annual blue water footprints of microalgal systems: whole wet biomass, algal proteins, and algal biofuels. Results represent the annual mean of 21 simulated years (1998-2018) using the computed water demands and biomass yields for a 400-ha facility.

In contrast, the WF of algal biofuels is significantly larger than petroleum-based diesel. Lampert et al. [66] reported a well-to-wheel water consumption of 1.54 m^3 GJ^{-1} for petroleum-based diesel. Even when comparing the most favorable WF of algal biodiesel, water consumption is five times higher than diesel. However, compared to other biodiesel feedstocks, algal biodiesel presents one of the most favorable water footprints. Gerbens-Leenes et al. [20] calculated a WF of 216 and 298 m^3 GJ^{-1} for soybean and rapeseed biodiesel, respectively. In the same way, the blue WF of ethanol from corn biomass was reported to be 37 m^3 GJ^{-1} [20]. When compared to algal biodiesel, even the most unfavorable scenario is more water-efficient than corn ethanol by 44%. The evident gap between the WF of biofuels and petroleum-based fuels is associated with the substantial irrigation requirements for biomass production. Microalgal biomass, different from terrestrial crops, is positioned between these systems regarding water consumption.

This assessment highlights the advantages of whole algal biomass, proteins, and fuels over first and second-generation energy crops from a water footprint perspective. It is also important to note that this comparison is based on national averages and that specific regional variations are not considered due to the lack of data for conventional systems. For example, maize outputs in the Midwest are much higher than the national average which might reduce the WF of maize production in this region. Similarly, the growth rate for algal systems in the Gulf Coast region is well above the national average resulting in a more favorable local WF in that specific region. Only the blue water footprints of conventional systems were compared to provide an objective evaluation among feedstocks, contributions from the green and gray WF components were neglected. In reality, conventional crops often have higher green and gray WF

components, while microalgae cultivation does not produce a green WF and the gray component is negligible if proper media recycling strategies are implemented [19].

However, the comparison to petroleum-based diesel demonstrates that algal biofuels are significantly more water-intensive than conventional diesel. It is important to note that the results discussed so far represent a local water withdrawal and do not include the WF of the full supply chain (well-to-wheel) of algal biofuel production. If the system boundary is expanded and the indirect water consumption from upstream processes is considered, the gap between conventional fuels and algal biofuels will further increase. The indirect WF of nutrients and electricity will vary regionally based on transportation requirements and electric generation technology and may represent a substantial contribution to the life cycle of water. However, the water consumption associated with the materials used in the hydrothermal liquefaction conversion process will increase the WF by 0.503 m^3 per GJ [67], demonstrating that water is primarily consumed through evaporation.

The WF of algal biofuels could be minimized through improvements in algal productivity or by considering seawater or brackish cultivation at locations with high water requirements. Additionally, co-production of high-value products or the incorporation of less water-intensive cultivation platforms such as closed photobioreactors could improve water usage metrics, although closed photobioreactors and covered ORPs may bring about more significant issues associated with exceeding algal temperature limits.

3.3.4 Temperature tolerance evaluation

The performance of commercial outdoor algae cultivation is heavily influenced by the thermal conditions of the culture. Since pond temperatures are also dependent on the magnitude of evaporative effects, co-modeling of pond temperatures and evaporation at a high temporal and

spatial resolution are needed to gain an accurate and in-depth understanding of temperature profiles of commercial-scale facilities. The computed pond temperatures for the entire simulation period were processed to analyze seasonal and geographical trends.

The maximum temperatures that a specific strain will tolerate to avoid culture failure for one hour are illustrated in Fig. 6. As it is readily visible in Fig. 6, the highest summer temperatures are observed in the southern latitudes, where temperatures exceed 40°C. The analysis was also extended to a maximum temperature exposure or tolerance of two and three hours. The average variation between the one-hour and two-hour temperature tolerance was 0.4°C. When comparing the one-hour and three-hour scenarios, a larger difference of 1.4°C was calculated. These results can support informed decisions on strain selection and facility siting. For example, a strain grown in Phoenix, AZ must have a one-hour temperature tolerance of 44.6 °C and tolerate temperatures above 43°C for three consecutive hours of culture exposure while a strain grown in Lexington, KY must tolerate a one-hour exposure of 38.9 °C and a three-hour temperature tolerance of 37.4 °C. All the calculated temperature tolerances are provided in the Appendix.

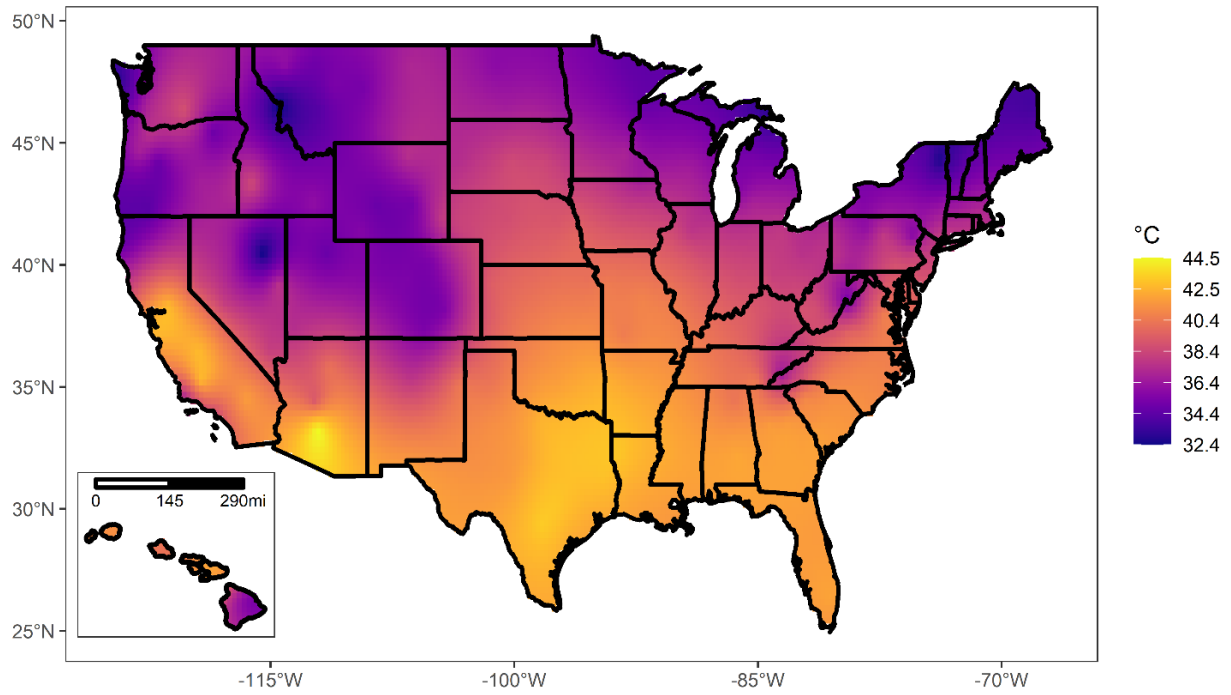

Figure 6. Mean maximum pond temperatures for the CONUS and Hawaii for a 400-ha facility. The illustrated temperatures are the one-hour temperature that must be tolerated to avoid culture crashing. Results represent the annual mean of 21 simulated years (1998-2018).

Although a marked distinction exists between the southwestern and Gulf Coast regions in terms of evaporation rates, this is not the case for their temperature profiles and a similar range of maximum temperatures was found in both regions. This difference is explained by examining the parameters with the highest impact on the heat fluxes which influence pond temperatures. Evaporation rates were highly sensitive to wind speeds and relative humidity conditions, similarly, temperature profiles are also influenced by ambient temperatures and solar radiation. For instance, ambient temperature is higher in the desert southwest, but the low relative humidity enhances evaporative cooling consequently decreasing pond temperatures. On the other hand, pond temperatures in the Gulf Coast region are closer to ambient conditions due to the high humid conditions in the region.

When expanding the facility size, a relatively low increase in temperatures was observed for results generated with both weather data sets. The average temperature difference between the 400-ha and 4000-ha using weather data from the NSRDB increased by 1 % (Fig. A25). Similarly, the difference for the TMY3 case was calculated to increase by 3 % (Fig. A28). These differences are correlated to the drop in evaporative cooling related to the change in surface area of the facility. Furthermore, results reflect that a relatively low error is introduced when computing temperature profiles with TMY3 data as opposed to the error observed in the prediction of water demands. The low variance is linked to the fact that TMY3 files do provide proper solar radiation and ambient temperature measurements, in contrast to wind speed data. The average temperature difference between the results generated with TMY3 and NSRDB weather data for a 400-ha and 4000-ha facility was calculated to be 4 % and 3 %, respectively (Fig. A31).

Additionally, a more in-depth seasonal and geographical assessment of pond temperatures was performed. Descriptive statistics of pond temperature data corresponding to five case studies spanning the 21-year simulated period are shown in Fig. 7. The seasonal variability results demonstrate the importance of high temporal resolution in temperature modeling. Results allow the identification of subtle differences among locations and seasons. The first thing to note is the similarities in temperature ranges but differences in the spread of temperatures when comparing Baton Rouge, Phoenix, and Tampa. For example, the median temperature during spring and summer at these three locations is approximately the same, but temperatures in Baton Rouge and Tampa are much closer to the median. Selecting strains with optimal temperatures around the median will have a more advantageous effect in Baton Rouge and Tampa than in Phoenix, where temperatures are more dispersed around the median. This is

demonstrated by the high productivity results from Lihue, where the range and dispersion are smaller than all the other locations for the four seasons and the seasonal variability is minimal.

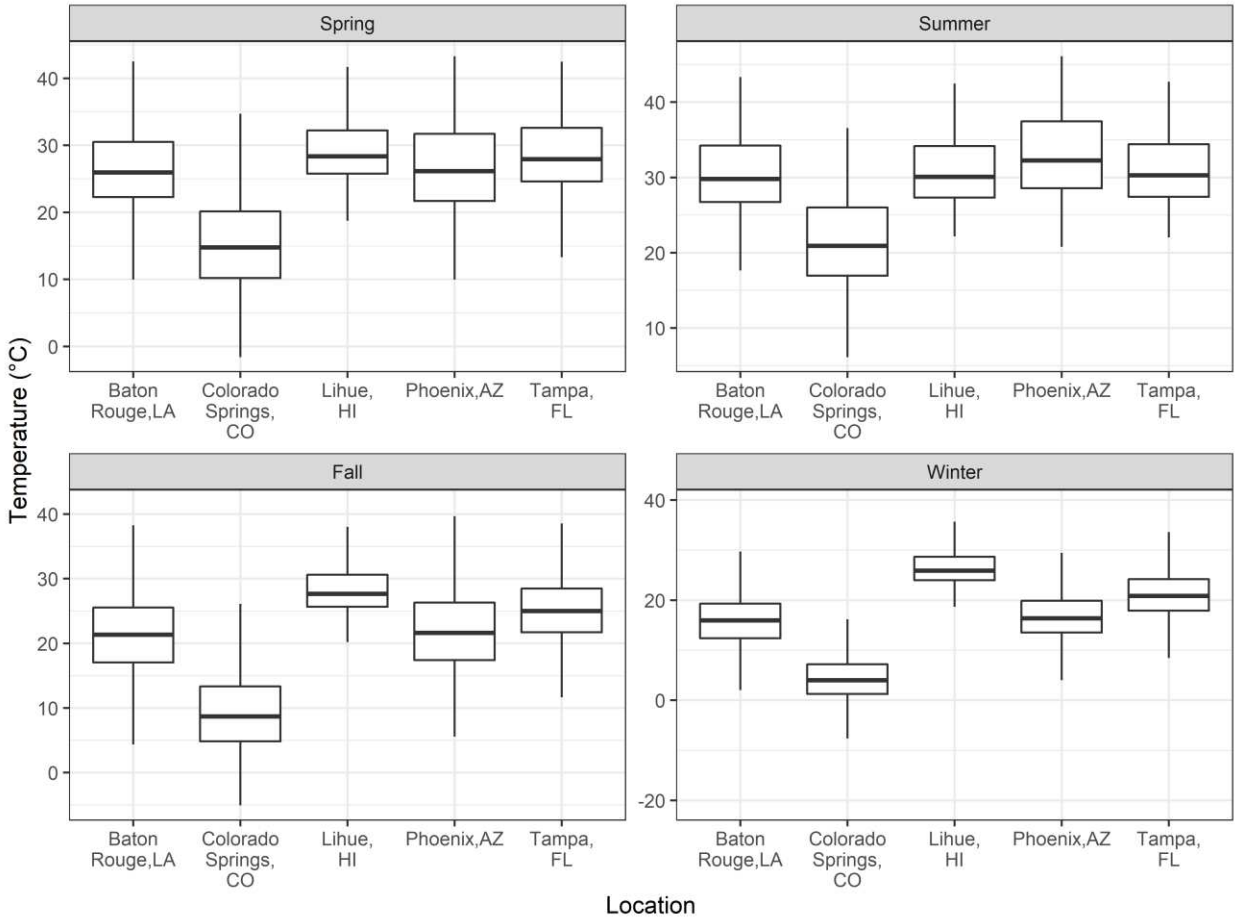

Figure 7. Mean seasonal temperature profiles for the 21-year simulation period for five distinct locations across the US. The boxes represent the interquartile range, outliers are not included.

Furthermore, when observing locations like Colorado Springs, temperatures during the spring, fall, and winter render open cultivation unproductive. Successful biomass cultivation at regions with this temperature profile will require the incorporation of temperature-regulated systems. Another alternative is varying the culture's depth as a temperature regulation strategy. This strategy is supported by the fact that the temperature in thinner cultures is significantly higher.

Results highlight the importance of temperature on the outdoor cultivation of biomass in ORPs. More importantly, the data indicates that the temperatures measured in elevated raceways are not representative of commercial-scale ORPs. The temperatures calculated in this study are significantly higher than those seen in experimental trials of elevated raceways [57]. Given the importance of temperature on algal growth, it is important to establish accurate temperature profiles of commercial ponds and understand the effects on the economics and operations of algal facilities. Future research will focus on the integration of these temperature profiles with strain-specific temperature crashing models to understand geographical differences in the operational days of algae facilities.

4. CONCLUSIONS

This study provides a robust assessment of the water demands of commercial-scale algae cultivation for conventional algae systems using a validated model with an average temperature predictive error of -0.96 ± 2.72 °C and evaporation accuracy of 1.46 ± 5.92 %. A validated biological model with an error of -4.59 ± 8.13 % was used to represent the current state of technology. The model was leveraged with historical weather data and WF methodologies to provide a temporal and geographical assessment of the water demands, temperature, and WF of algal biomass, proteins, and biodiesel. Results highlight the interactions between geographic inputs and facility sizes on temperature profiles and water demands of algae farms. Accurate prediction of evaporation rates requires high-quality weather data, specifically wind speed measurements, while the temperature profiles are more sensitive to temperature and solar radiation parameters. Appropriate selection of the evaporation model is of equal importance as the evaporation model must capture the effects of pond size to reduce the uncertainty in these calculations. This study also incorporates a novel outlook on the temperature tolerances needed for cultivation in commercial-scale open systems. Using current biomass production and conversion technologies, the national average of the blue WF of algal biomass, proteins, and fuels was calculated to be 157 m^3 water $tonne^{-1}$ AFDW biomass, 376 m^3 water $tonne^{-1}$ algal proteins, and 11.2 m^3 GJ^{-1} biofuel, respectively. The WF of algal systems was found to be more favorable when compared to conventional biomass feedstocks. However, improvements are still needed to achieve a smaller WF than petroleum-based fuels. Moving forward, cultivation in saline media may be an attractive solution to reduce these WF, but a better understanding of the implications on temperature and growth, as well as economical aspects, is required.

4.1 Future Work

The modeling results presented in this study provide a robust foundation for future commercial-scale modeling and optimization of algal facilities. Results can be further integrated with sustainability modeling to determine the economic viability and environmental impacts of algal cultivation at a specific location. The high spatiotemporal resolution model allows for a complete resource assessment based on land availability at a county level and minimizing the distance to carbon sources.

The coupling of the model with historical weather data and strain-specific parameters allows for a comprehensive analysis of the thermal dynamics and productivity potential of a large-scale facility. Future work could focus on performing multi-objective optimization based on seasonal strain rotation and depth variation. The operating pond depth has a major influence on the thermal behavior of the system and operating at an optimal depth, that maintains culture temperature near the strain-specific optimal temperature, could potentially increase biomass yields.

In addition, a better understanding of the temperature limits for freshwater cultivation is required. The current state of the growth model does not capture second-order effects that high temperatures could trigger such as higher contamination rates. Frequent pond crashing will increase facility downtime and might require the implementation of crop protection strategies, which will negatively impact the economics of algal systems. Future efforts might include incorporating pond reliability data and validating the model with high-temperature tolerant strains will improve the biological model's ability to predict growth rates of commercial algae ponds.

Moreover, the proposed water footprint assessment could be expanded into a comprehensive water life-cycle study. The consumptive water from upstream processes in the algal supply such as electricity generation and nutrient production will increase the water footprint of algal systems and comparing this metric to other energy crops is essential for future research and development. The high resolution of the model allows for a thorough examination of the variation of water consumption by accounting for the consumptive water of transportation of nutrients or regional electric grids. Expanding the system boundary to include different conversion pathways and assessed them based on water consumption will be a future area of focus.

Finally, future work could also examine the impact of saline cultivation on water consumption metrics. Saline cultivation will require a detailed accounting of salt concentration on the system and could potentially increase energy metrics through salt blowdown disposal. Blowdown requirements will vary regionally, being higher in areas with high evaporation rates and could represent significant economic penalties on the costs of biomass production. However, saline cultivation could be beneficial from the water footprint perspective and the trade-offs must be carefully assessed at a seasonal and regional level.

REFERENCES

[1] U.S. DOE 2010., "National Algal Biofuels Technology Roadmap."

[2] Y. Chisti, "Biodiesel from microalgae," *Biotechnology Advances*, vol. 25, no. 3. Elsevier, pp. 294–306, 01-May-2007.

[3] A. L. Ahmad, N. H. M. Yasin, C. J. C. Derek, and J. K. Lim, "Microalgae as a sustainable energy source for biodiesel production: A review," *Renewable and Sustainable Energy Reviews*, vol. 15, no. 1. Pergamon, pp. 584–593, 01-Jan-2011.

[4] A. F. Clarens, E. P. Resurreccion, M. A. White, and L. M. Colosi, "Environmental life cycle comparison of algae to other bioenergy feedstocks," *Environ. Sci. Technol.*, vol. 44, no. 5, pp. 1813–1819, 2010.

[5] Z. Liu, C. Liu, S. Han, and X. Yang, "Optimization upstream CO2 deliverable with downstream algae deliverable in quantity and quality and its impact on energy consumption," *Sci. Total Environ.*, vol. 709, p. 136197, Mar. 2020.

[6] A. H. Alami, S. Alasad, M. Ali, and M. Alshamsi, "Investigating algae for CO2 capture and accumulation and simultaneous production of biomass for biodiesel production," *Sci. Total Environ.*, vol. 759, p. 143529, Mar. 2021.

[7] Z. Chi, Y. Xie, F. Elloy, Y. Zheng, Y. Hu, and S. Chen, "Bicarbonate-based Integrated Carbon Capture and Algae Production System with alkalihalophilic cyanobacterium," *Bioresour. Technol.*, vol. 133, pp. 513–521, Apr. 2013.

[8] B. R. Kumar *et al.*, "A state of the art review on the cultivation of algae for energy and other valuable products: Application, challenges, and opportunities," *Renewable and Sustainable Energy Reviews*, vol. 138. Elsevier Ltd, p. 110649, 01-Mar-2021.

[9] B. D. Beckstrom, M. H. Wilson, M. Crocker, and J. C. Quinn, "Bioplastic feedstock production from microalgae with fuel co-products: A techno-economic and life cycle impact assessment," *Algal Res.*, vol. 46, p. 101769, Mar. 2020.

[10] A. Kusmayadi, Y. K. Leong, H.-W. Yen, C.-Y. Huang, and J.-S. Chang, "Microalgae as sustainable food and feed sources for animals and humans – biotechnological and environmental aspects," *Chemosphere*, vol. 271, p. 129800, Jan. 2021.

[11] T. C. Adarme-Vega, D. K. Y. Lim, M. Timmins, F. Vernen, Y. Li, and P. M. Schenk, "Microalgal biofactories: a promising approach towards sustainable omega-3 fatty acid production," *Microbial Cell Factories*, vol. 11. 25-Jul-2012.

[12] M. L. N. M. Carneiro *et al.*, "Potential of biofuels from algae: Comparison with fossil fuels, ethanol and biodiesel in Europe and Brazil through life cycle assessment (LCA)," *Renewable and Sustainable Energy Reviews*, vol. 73. Elsevier Ltd, pp. 632–653, 01-Jun-2017.

[13] A. Singh, P. S. Nigam, and J. D. Murphy, “Renewable fuels from algae: An answer to debatable land based fuels,” *Bioresour. Technol.*, vol. 102, no. 1, pp. 10–16, Jan. 2011.

[14] M. S. Wigmosta, A. M. Coleman, R. J. Skaggs, M. H. Huesemann, and L. J. Lane, “National microalgae biofuel production potential and resource demand,” *Water Resour. Res.*, vol. 47, no. 4, pp. 1–13, 2011.

[15] J. C. Quinn, K. B. Catton, S. Johnson, and T. H. Bradley, “Geographical Assessment of Microalgae Biofuels Potential Incorporating Resource Availability,” *Bioenergy Res.*, vol. 6, no. 2, pp. 591–600, 2013.

[16] M. D. Somers and J. C. Quinn, “Sustainability of carbon delivery to an algal biorefinery: A techno-economic and life-cycle assessment,” *J. CO2 Util.*, 2019.

[17] R. E. Davis *et al.*, “2017 Algae Harmonization Study: Evaluating the Potential for Future Algal Biofuel Costs, Sustainability, and Resource Assessment from Harmonized Modeling,” Golden, CO (United States), Aug. 2018.

[18] B. Guieysse, Q. Béchet, and A. Shilton, “Variability and uncertainty in water demand and water footprint assessments of fresh algae cultivation based on case studies from five climatic regions,” *Bioresour. Technol.*, vol. 128, pp. 317–323, Jan. 2013.

[19] P. W. Gerbens-Leenes, L. Xu, G. J. de Vries, and A. Y. Hoekstra, “The blue water footprint and land use of biofuels from algae,” *Water Resour. Res.*, vol. 50, no. 11, pp. 8549–8563, Nov. 2014.

[20] P. W. Gerbens-Leenes, A. Y. Hoekstra, and T. H. Van Der Meer, “The water footprint of bio-energy: Global Water Use for Bio-Ethanol, Bio-Diesel, Heat and Electricity,” *Value Water Res. Rep. Ser.*, vol. 34, no. 34, p. 108, 2008.

[21] M. Q. Frank, Edward D., Han, J., Palou-Rivera, I., Elgowainy, A., Wang, “Life-Cycle Analysis of Algal Lipid Fuels with the GREET Model,” 2011.

[22] J. Yang, M. Xu, X. Zhang, Q. Hu, M. Sommerfeld, and Y. Chen, “Life-cycle analysis on biodiesel production from microalgae: Water footprint and nutrients balance,” *Bioresour. Technol.*, vol. 102, no. 1, pp. 159–165, Jan. 2011.

[23] J. W. Moody, C. M. McGinty, and J. C. Quinn, “Global evaluation of biofuel potential from microalgae,” *Proc. Natl. Acad. Sci. U. S. A.*, vol. 111, no. 23, pp. 8691–8696, Jun. 2014.

[24] K. Sander and G. S. Murthy, “Life cycle analysis of algae biodiesel,” *Int. J. Life Cycle Assess.*, vol. 15, no. 7, pp. 704–714, Aug. 2010.

[25] Q. Béchet, B. Sialve, J. P. Steyer, A. Shilton, and B. Guieysse, “Comparative assessment of evaporation models in algal ponds,” *Algal Res.*, vol. 35, no. June, pp. 283–291, 2018.

[26] J. C. Greene, Jonah M., Quiroz, David, Compton, Sam, Lammers, Peter J., Quinn, “A validated thermal and biological model for predicting algal productivity in large scale outdoor cultivation systems,” *Algal Res.*, 2021.

[27] K. Friedrich *et al.*, “Reservoir evaporation in the Western United States,” *Bull. Am.*

Meteorol. Soc., vol. 99, no. 1, pp. 167–187, 2018.

[28] K. R. Helfrich, E. E. Adams, A. L. Godbey, and D. R. F. Harleman, "Evaluation of Models for Predicting Evaporative Water Loss in Cooling Impoundments," *Report*, no. March, p. 164, 1982.

[29] E. Sartori, "A critical review on equations employed for the calculation of the evaporation rate from free water surfaces," *Sol. Energy*, vol. 68, no. 1, pp. 77–89, 2000.

[30] K. D. Ryan, Patrick J, Harleman, Donald R.F., Stolzenbach, "Surface Heat Loss From Cooling Ponds," *Water Resour. Res.*, vol. 16, no. 5, 1974.

[31] E. E. Adams, D. J. Cosler, and K. R. Helfrich, "Evaporation from heated water bodies: Predicting combined forced plus free convection," *Water Resour. Res.*, vol. 26, no. 3, pp. 425–435, 1990.

[32] C. Quiroz-Arita *et al.*, "A dynamic thermal algal growth model for pilot-scale open-channel raceways," *Bioresour. Technol. Reports*, vol. 10, no. February, p. 100405, 2020.

[33] G. Khawam, P. Waller, S. Gao, S. Edmundson, M. S. Wigmosta, and K. Ogden, "Model of temperature, evaporation, and productivity in elevated experimental algae raceways and comparison with commercial raceways," *Algal Res.*, vol. 39, p. 101448, May 2019.

[34] R. L. White and R. A. Ryan, "Long-Term Cultivation of Algae in Open-Raceway Ponds: Lessons from the Field," *Ind. Biotechnol.*, vol. 11, no. 4, pp. 213–220, 2015.

[35] S. Wilcox and W. Marion, "Users manual for TMY3 data sets," *Renew. Energy*, 2008.

[36] A. Y. Hoekstra, A. K. Chapgain, M. M. Aldaya, and M. M. Mekonnen, *The Water Footprint Assessment Manual*. London: Earthscan, 2011.

[37] T. L. Bergman, A. S. Lavine, F. P. Incropera, and D. P. Dewitt, *Fundamentals of Heat and Mass Transfer*, 7th ed. John Wiley & Sons, Ltd, 2011.

[38] D. Brunt, "Notes on radiation in the atmosphere. I," *Q. J. R. Meteorol. Soc.*, vol. 58, no. 247, pp. 389–420, Oct. 1932.

[39] A. Q. Béchet, A. Shilton, J. B. K. Park, R. J. Craggs, and B. Guieysse, "Universal temperature model algal ponds," 2010.

[40] J. Lamoureux, T. R. Tiersch, and S. G. Hall, "Pond heat and temperature regulation (PHATR): Modeling temperature and energy balances in earthen outdoor aquaculture ponds," *Aquac. Eng.*, vol. 34, no. 2, pp. 103–116, Mar. 2006.

[41] J. R. Lloyd and W. R. Moran, "Natural Convection Adjacent To Horizontal Surface of Various Planforms.," *Am. Soc. Mech. Eng.*, no. 74-WA/HT-66, pp. 443–447, 1974.

[42] Q. Béchet, A. Shilton, J. B. K. Park, R. J. Craggs, and B. Guieysse, "Universal temperature model for shallow algal ponds provides improved accuracy," *Environ. Sci. Technol.*, vol. 45, no. 8, pp. 3702–3709, 2011.

[43] M. Sengupta, Y. Xie, A. Lopez, A. Habte, G. Maclaurin, and J. Shelby, "The National Solar Radiation Data Base (NSRDB)," *Renewable and Sustainable Energy Reviews*, vol.

89. Elsevier Ltd, pp. 51–60, 01-Jun-2018.

[44] J. R. Benemann, R. P. Goebel, J. C. Weissman, and D. C. Augenstein, “Microalgae as a source of liquid fuels. Final technical report. [200 references],” May 1982.

[45] J. R. Benemann and W. J. Oswald, “Systems and economic analysis of microalgae ponds for conversion of CO{sub 2} to biomass. Final report,” Pittsburgh, PA, and Morgantown, WV, Mar. 1996.

[46] T. J. Lundquist, I. Woertz, N. W. T. Quinn, and J. R. Benemann, “A Realistic Technology and Engineering Assessment of Algae Biofuel Production,” 2010.

[47] R. Davis *et al.*, “Renewable Diesel from Algal Lipids: An Integrated Baseline for Cost, Emissions, and Resource Potential from a Harmonized Model,” 2012.

[48] R. Davis *et al.*, “Process Design and Economics for the Conversion of Lignocellulosic Biomass to Hydrocarbons: Dilute-Acid and Enzymatic Deconstruction of Biomass to Sugars and Catalytic Conversion of Sugars to Hydrocarbons,” no. March, p. 133, 2015.

[49] S. Jones, Y. Zhu, D. Anderson, R. T. Hallen, and D. C. Elliott, “Process Design and Economics for the Conversion of Algal Biomass to Hydrocarbons : Whole Algae Hydrothermal Liquefaction and Upgrading,” 2014.

[50] R. Davis and L. Laurens, “Algal Biomass Production via Open Pond Algae Farm Cultivation: 2019 State of Technology and Future Research,” no. April, pp. 1–32, 2020.

[51] J. R. Cruce and J. C. Quinn, “Economic viability of multiple algal biorefining pathways and the impact of public policies,” *Appl. Energy*, vol. 233–234, pp. 735–746, Jan. 2019.

[52] E. D. Frank, A. Elgowainy, J. Han, and Z. Wang, “Life cycle comparison of hydrothermal liquefaction and lipid extraction pathways to renewable diesel from algae,” *Mitig. Adapt. Strateg. Glob. Chang.*, vol. 18, no. 1, pp. 137–158, Jan. 2013.

[53] F. W. T. Penning De Vries, D. M. Jansen, H. F. M. Ten Berge, and A. Bakema, “Simulation of ecophysiological processes of growth in several annual crops.”

[54] a K. Chapagain and a Y. Hoekstra, “Water Footprints of Nations (Vol 2),” *Water Res.*, vol. 2, no. 16, p. 240, 2004.

[55] B. E. Dale, “Biomass Refining: Protein and Ethanol from Alfalfa,” *Ind. Eng. Chem. Prod. Res. Dev.*, vol. 22, no. 3, pp. 466–472, 1983.

[56] R. J. Henry, “THE CARBOHYDRATES OF BARLEY GRAINS - A REVIEW,” *J. Inst. Brew.*, vol. 94, no. 2, pp. 71–78, Mar. 1988.

[57] J. McGowen *et al.*, “The Algae Testbed Public-Private Partnership (ATP3) framework; establishment of a national network of testbed sites to support sustainable algae production,” *Algal Res.*, vol. 25, pp. 168–177, Jul. 2017.

[58] L. Rodolfi *et al.*, “Microalgae for oil: Strain selection, induction of lipid synthesis and outdoor mass cultivation in a low-cost photobioreactor,” *Biotechnol. Bioeng.*, vol. 102, no. 1, pp. 100–112, Jan. 2009.

[59] E. R. Venteris, R. C. Mcbride, A. M. Coleman, R. L. Skaggs, and M. S. Wigmosta, "Siting Algae Cultivation Facilities for Biofuel Production in the United States: Trade-Offs between Growth Rate, Site Constructability, Water Availability, and Infrastructure," 2014.

[60] V. L. Harmon *et al.*, "Reliability metrics and their management implications for open pond algae cultivation," *Algal Res.*, vol. 55, p. 102249, May 2021.

[61] C. Quiroz-Arita *et al.*, "A dynamic thermal algal growth model for pilot-scale open-channel raceways," *Bioresour. Technol. Reports*, vol. 10, p. 100405, Jun. 2020.

[62] N. Sun, R. L. Skaggs, M. S. Wigmosta, A. M. Coleman, M. H. Huesemann, and S. J. Edmundson, "Growth modeling to evaluate alternative cultivation strategies to enhance national microalgal biomass production," *Algal Res.*, vol. 49, p. 101939, Aug. 2020.

[63] C. F. Dewes, I. Rangwala, J. J. Barsugli, M. T. Hobbins, and S. Kumar, "Drought risk assessment under climate change is sensitive to methodological choices for the estimation of evaporative demand," *PLoS One*, vol. 12, no. 3, p. e0174045, Mar. 2017.

[64] J. R. Cruce *et al.*, "Driving toward sustainable algal fuels: A harmonization of techno-economic and life cycle assessments," *Algal Research*, vol. 54. Elsevier B.V., p. 102169, 01-Apr-2021.

[65] R. Davis *et al.*, "Process Design and Economics for the Conversion of Algal Biomass to Biofuels: Algal Biomass Fractionation to Lipid- and Carbohydrate-Derived Fuel Products," 2013.

[66] D. J. Lampert, H. Cai, and A. Elgowainy, "Wells to wheels: Water consumption for transportation fuels in the United States," *Energy Environ. Sci.*, vol. 9, no. 3, pp. 787–802, Mar. 2016.

[67] GREET, "GREET Life Cycle Model User Guide," *Argonne Natl. Labratory*, pp. 169–232, 2020.

[68] M. E. Martínez, J. M. Jiménez, and F. El Yousfi, "Influence of phosphorus concentration and temperature on growth and phosphorus uptake by the microalga Scenedesmus obliquus," *Bioresour. Technol.*, vol. 67, no. 3, pp. 233–240, Mar. 1999.

APPENDIX A

A1. Thermal model

This section describes the additional heat fluxes that are included in the thermal model and the methods used to calculate heat and mass transfer from forced convection. These heat fluxes were adopted directly from Greene et al. [1].

A1.1 Direct and diffuse solar radiation

The heat transfer from incoming solar radiation from both direct and diffuse components is modeled using the following equation:

$$Q_{solar} = (1 - f_a) \cdot GHI \cdot \alpha_{culture} \cdot A_s \quad \text{(A1)}$$

where $f_a = 0.015$ is the fraction of sunlight converted into chemical energy by the algae during photosynthesis, GHI [W m^{-2}] is the global horizontal irradiance, $\alpha_{culture}$ is the absorptivity of the algae culture set to 0.90, and A_s [m^2] is the pond surface area.

A1.2 Pond radiation

Radiation emitted by the pond was calculated using the following equation:

$$Q_{reradiation} = -\sigma \cdot \varepsilon_w \cdot T_p^4 \cdot A_s \quad \text{(A2)}$$

where ε_w is the emissivity of the culture with a calibrated value of 0.87, T_p is the pond temperature, and σ is the Stefan-Boltzmann constant.

A1.3 Inflow

Heat transfer from incoming water is calculated using the following equation:

$$Q_{inflow} = c_p \cdot m_e \cdot (T_{amb} - T_p) \quad \text{(A3)}$$

where c_p is the specific heat of the culture set to 4184 [J kg^{-1} K^{-1}], and m_e is the water loss from evaporation [kg m^{-2} s^{-1}].

A1.4 Heat transfer by forced convection

Heat transfer from forced convection is calculated using the flat plate correlations described in Bergman et al. [2]:

$$Nu_L = a \cdot (Re_L)^{0.5}(Pr)^{\frac{1}{3}} \qquad \text{for } Re_L < (3 \times 10^5) \text{ (Laminar Flow)} \quad \text{(A4)}$$

$$Nu_L = b \cdot (Re_L)^{0.8}(Pr)^{\frac{1}{3}} \qquad \text{for } Re_L > (5 \times 10^5) \text{ (Turbulent Flow)} \quad \text{(A5)}$$

$$Q_{convection} = h_{conv} \cdot (T_{amb} - T_{pond}) \quad \text{(A6)}$$

where a and b are empirical coefficients set to 0.75 and 0.015, respectively, h_{conv} [W m^{-2} K^{-1}] is the convection coefficient, Re_L is the Reynolds number, and Pr is the Prandtl number.

A2. Thermal validation

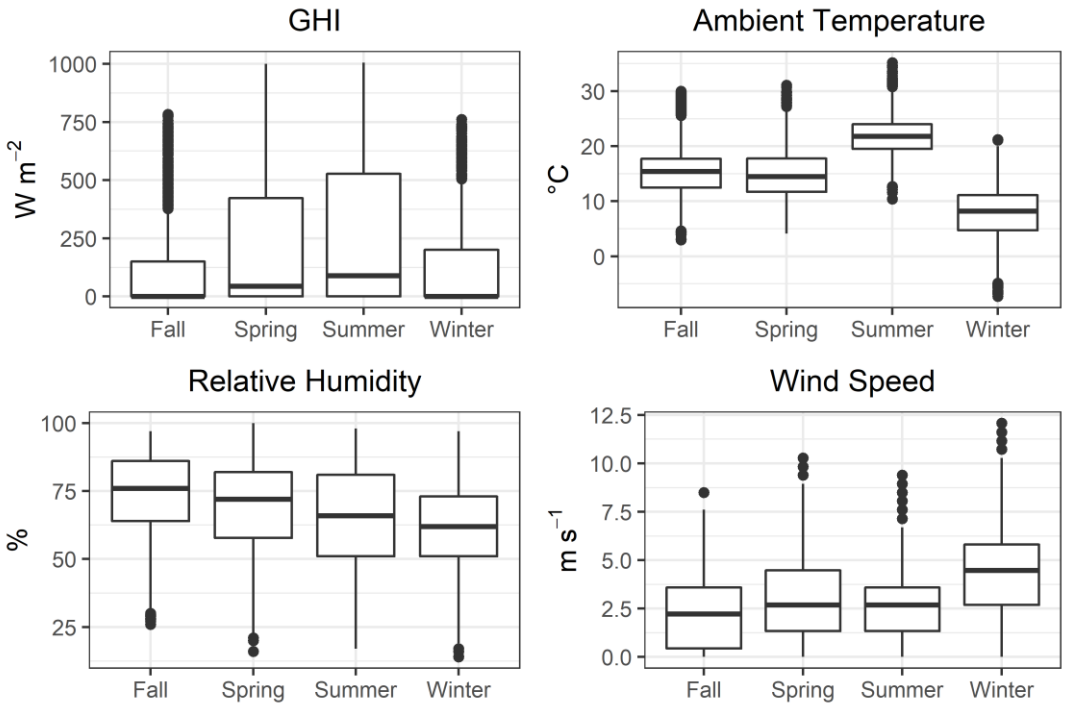

Figure A1. Seasonal inputs used in the thermal model validation effort.

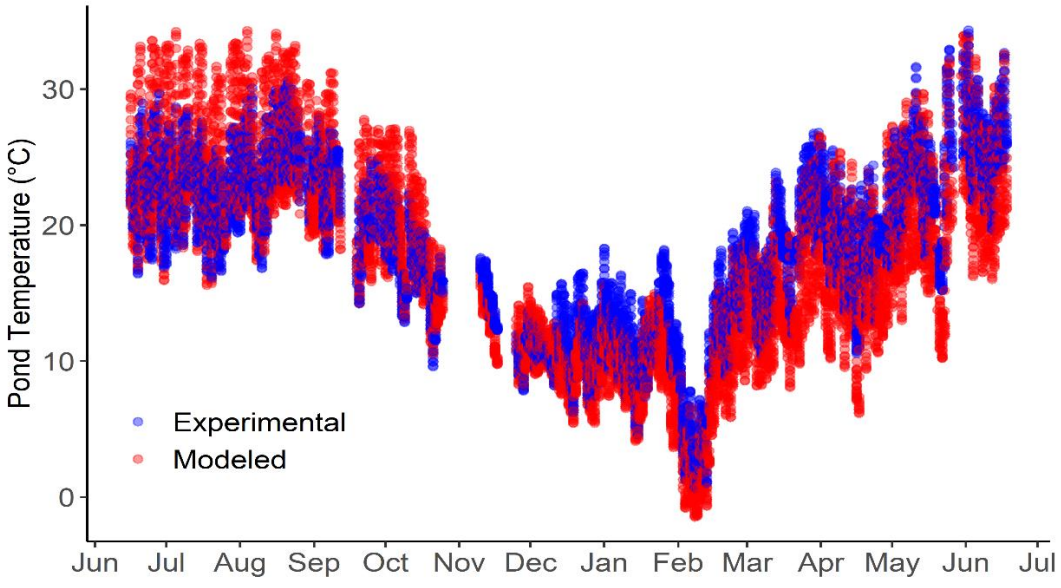

Figure A2. Time-series of the modeled and experimental pond temperature.

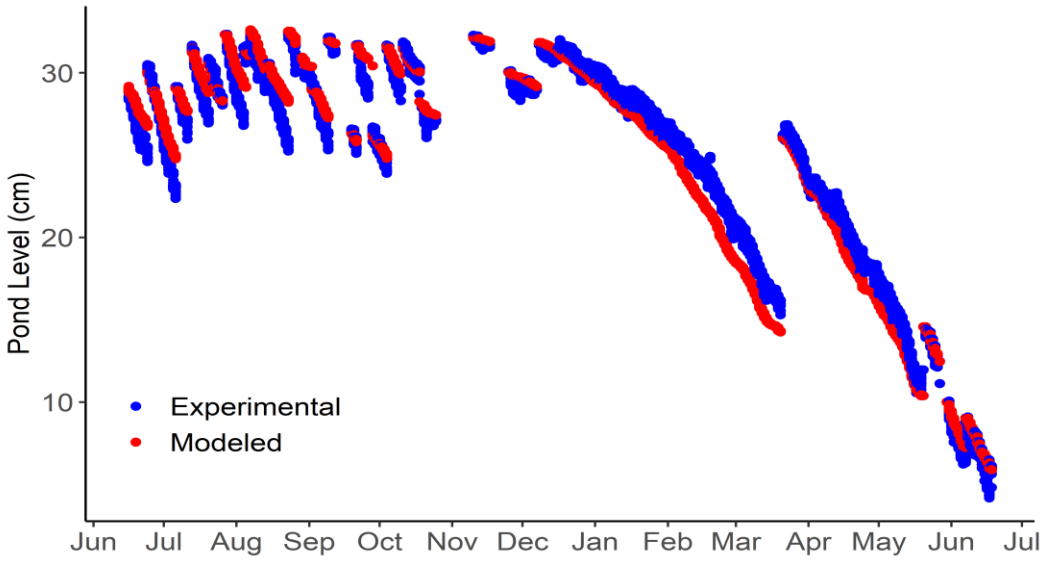

Figure A3. Time-series of the modeled and experimental pond depths.

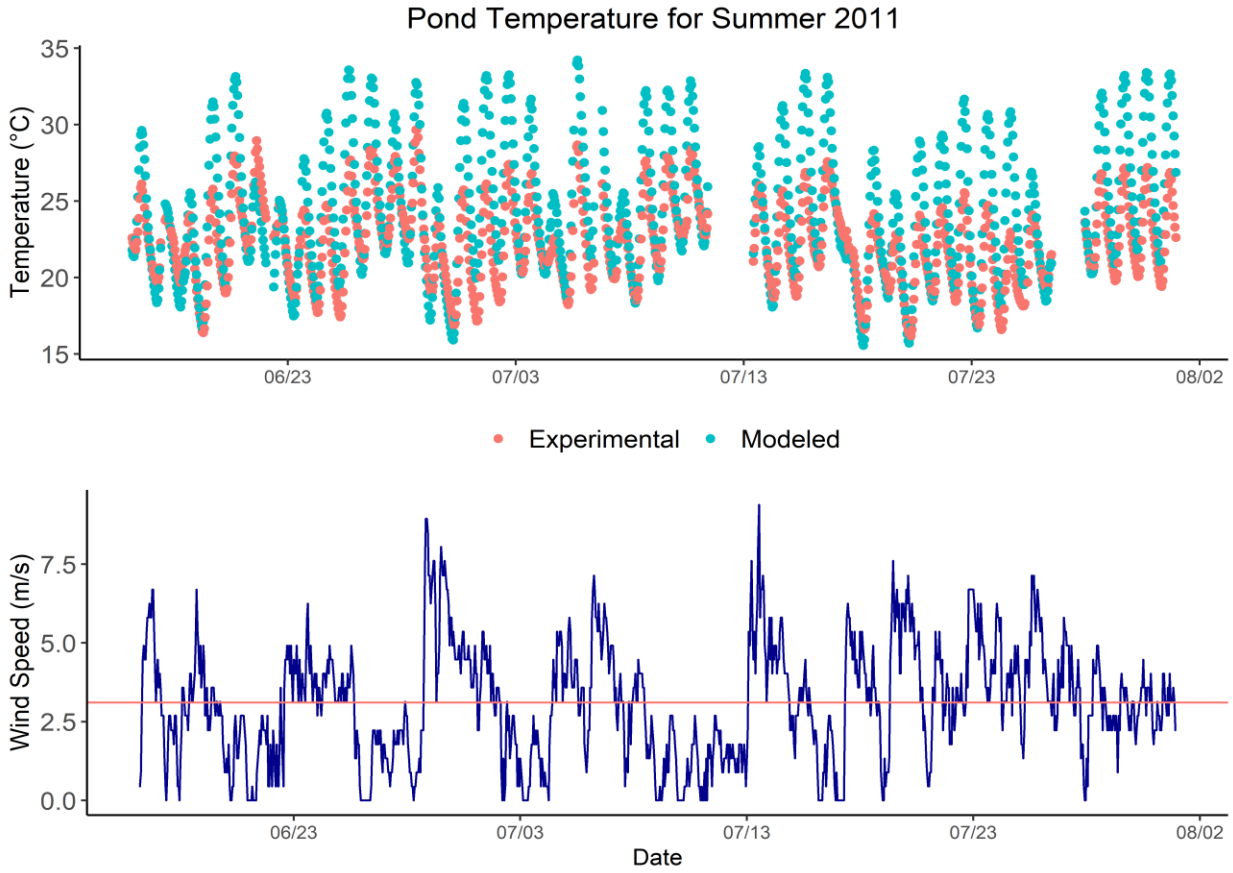

Figure A4. Relation between wind speed and pond temperature for Summer 2011. Gaps in the temperature series represent discarded time intervals. The red line denotes the mean wind speed for the period.

Table A2. Seasonal breakdown of the validation error.

	TEMPERATURE ERROR (°C)		EVAPORATION ERROR (%)	
SEASON	**Average**	**SD**	**Average**	**SD**
WINTER	-2.19	1.47	5.69	3.71
SPRING	-2.75	2.32	3.18	6.51
SUMMER	1.48	2.41	-3.24	4.7
FALL	0.46	1.85	-1.15	1.97

A3. Growth validation

The model inputs used for the validation of the growth model are tabulated below.

Table A3. Growth model inputs.

UTEX 393 Strain Parameters			
Parameter	**Value**	**Units**	**Source**
Optimal temperature	32.25	°C	[3]
Maximum temperature	40.9	°C	Empirical adjustment
Minimum temperature	3	°C	Empirical adjustment
Dark loss	3	%	Empirical adjustment
Saturation Light Intensity	480	$\mu\, mol\ m^{-2}\ s^{-1}$	Calibrated based on other summer strains
Optical Density Coefficient	0.38	g/L*OD750	AzCATI

A4. WF of first- and second-generation energy crops

Table A4. Blue WF of primary and secondary energy crops

Crop	*WF (m^3 per ton of crop)*	*Source*
Sugar beet	73	[4]
Alfalfa	124	[5]
Sugar cane	166	[4]
Maize	374	[4]
Barley	816	[4]
Sorghum	998	[4]
Soybean	1384	[4]

Table A5. Protein content primary and secondary energy crops

Crop	*Protein Content (g protein/g crop)*	*Source*
Sugar beet	0.05	[6]
Alfalfa	0.18	[7]
Sugar cane	0.07	[6]
Maize	0.08	[6]
Barley	0.11	[8]
Sorghum	0.09	[6]
Soybean	0.37	[6]

Table A6. WF of fuels.

Fuel	*WF (m^3 per GJ)*	*Source*
Soybean Biodiesel	*216*	[5]
Rapeseed Biodiesel	*298*	[5]
Diesel	*1.54*	[9]
Corn ethanol	*37*	[5]

A5. Dynamic maps of water demand

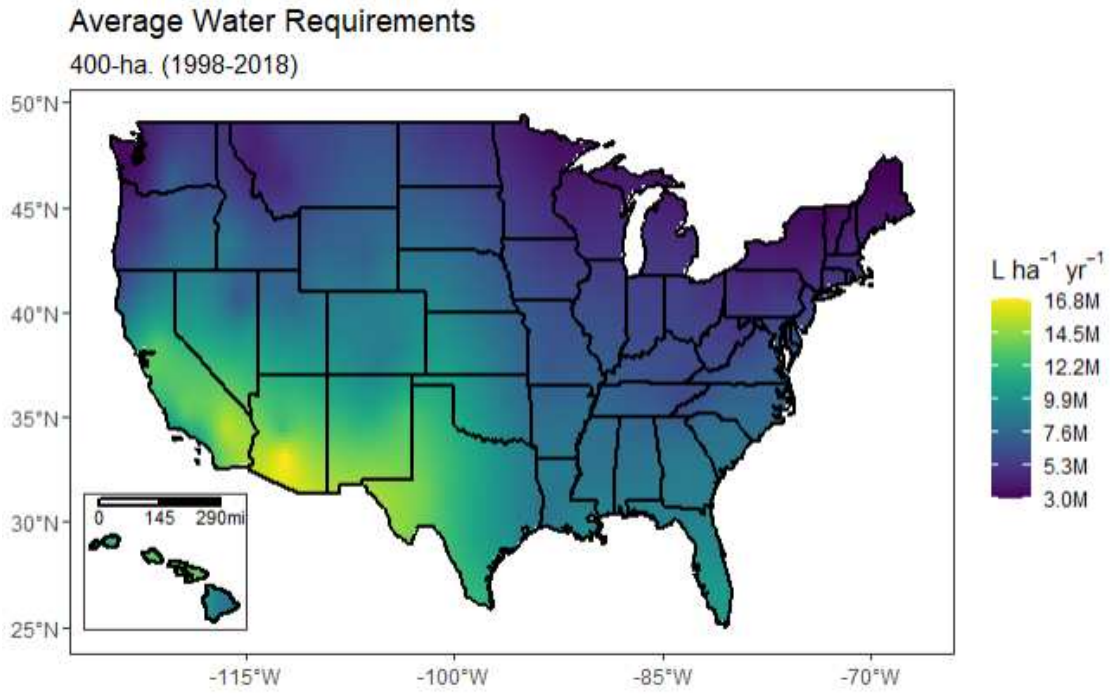

Figure A5. Mean annual water demand (L ha^{-1} yr^{-1}) for a 400-ha for the simulated 21 years.

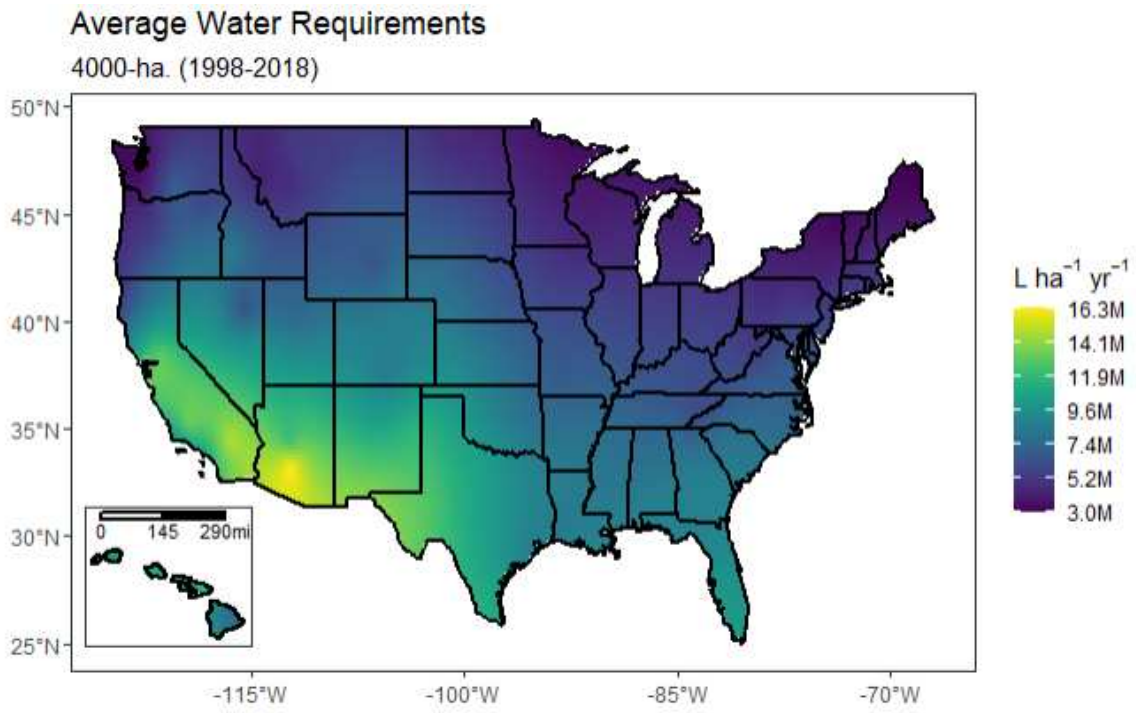

Figure A6. Mean annual water demand (L ha^{-1} yr^{-1}) for a 4000-ha for the simulated 21 years.

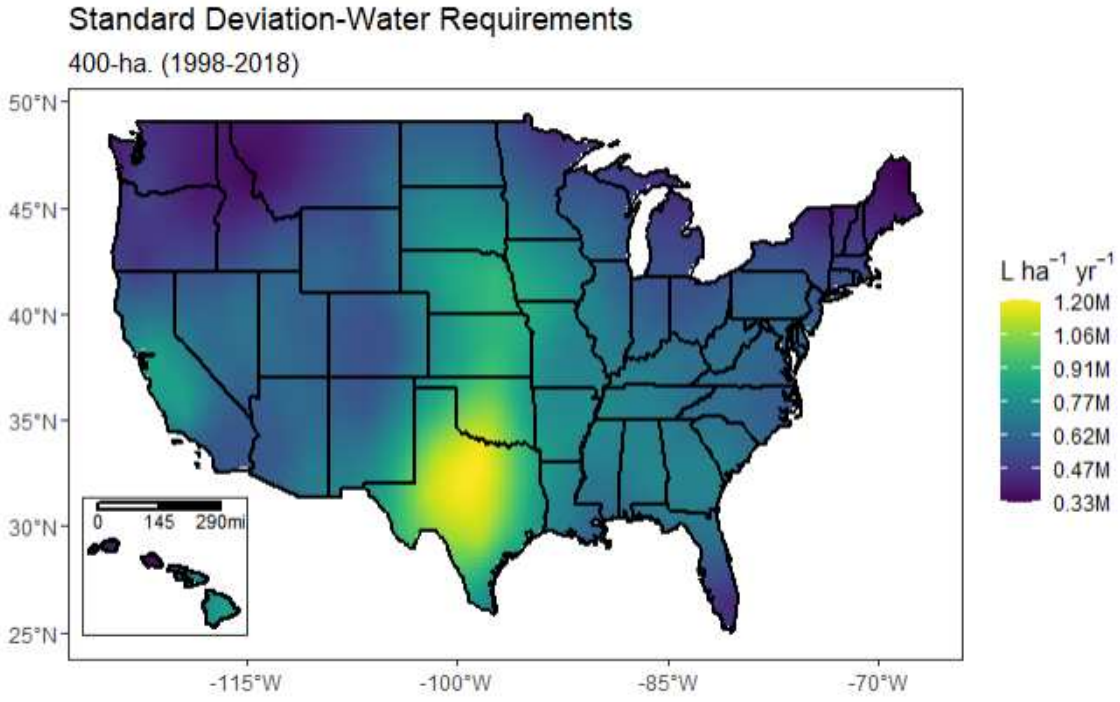

Figure A7. Standard deviation of annual water demand (L ha^{-1}) for a 400-ha algae farm for the simulated 21 years.

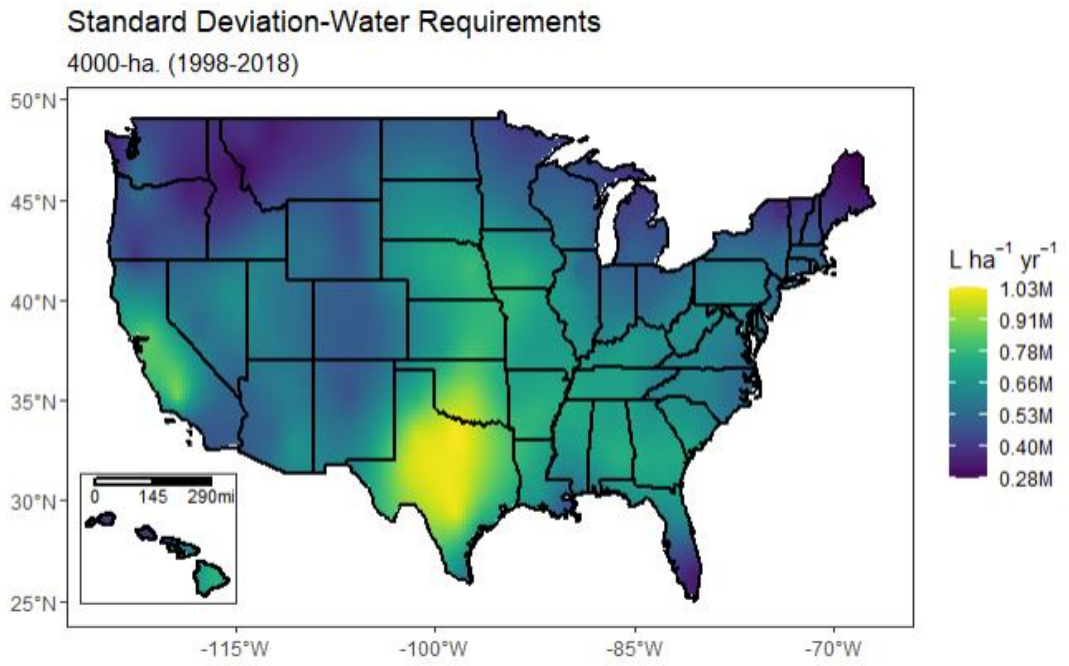

Figure A8. Standard deviation of annual water demand (L ha^{-1}) for a 400-ha algae farm for the simulated 21 years

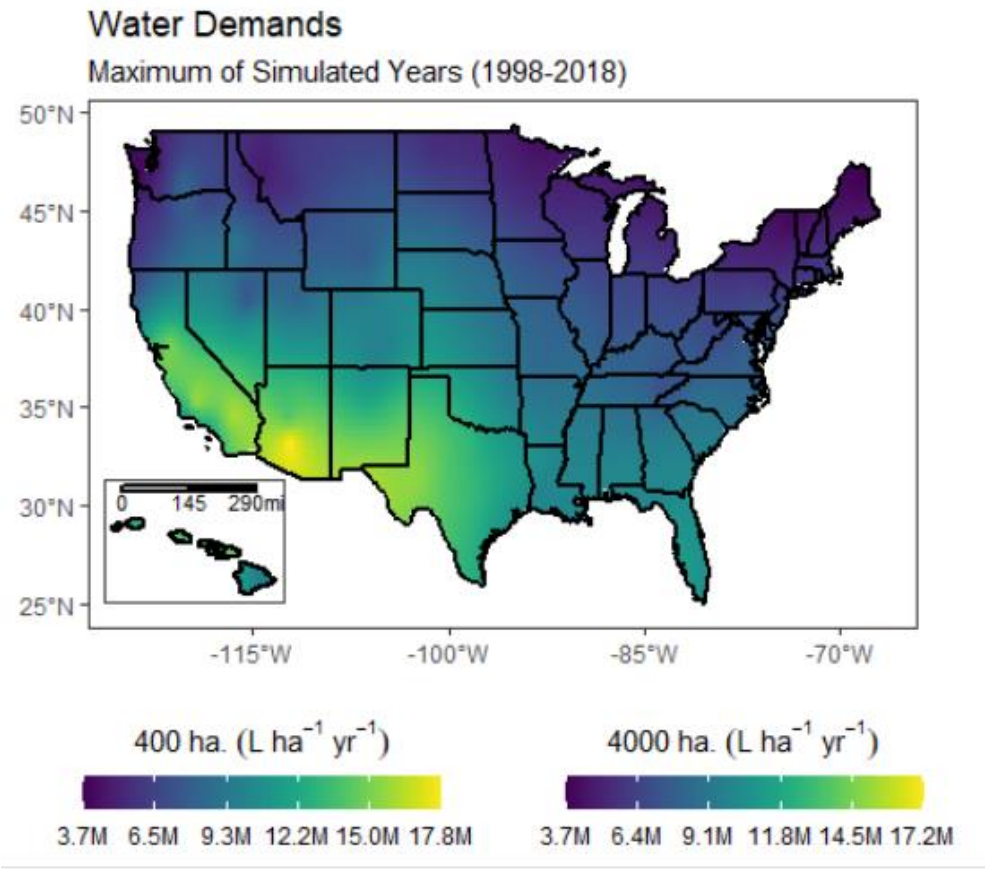

Figure A9. Maximum annual water demands (L ha^{-1} yr^{-1}) for the 400-ha and 4000-ha facilities for the 21 simulated years.

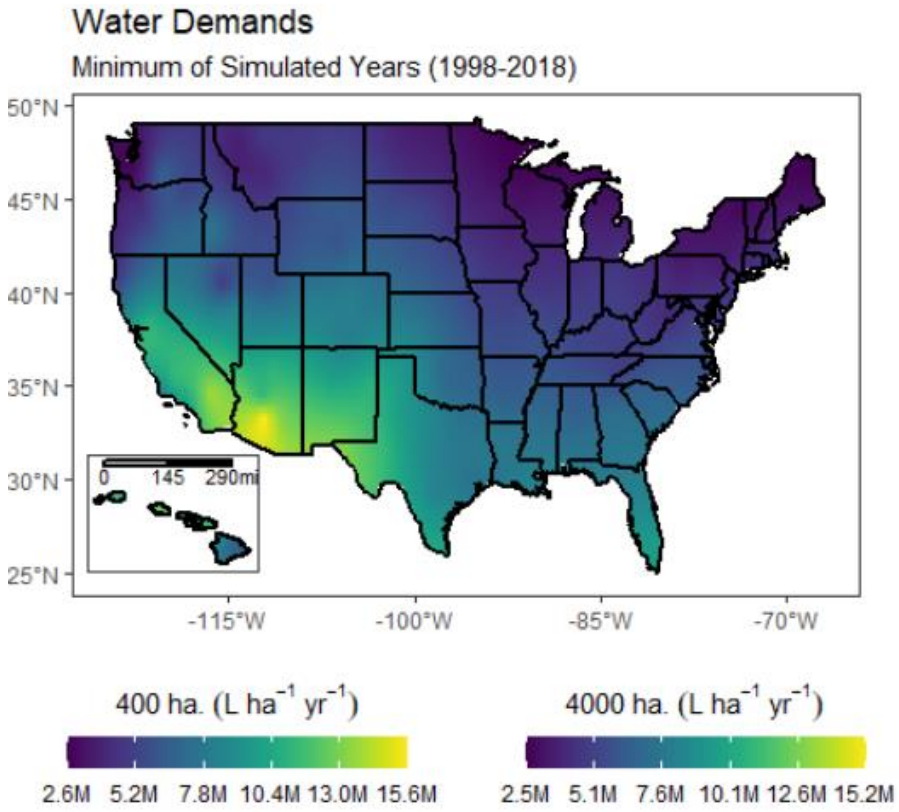

Figure A10. Maximum annual water demands (L ha^{-1} yr^{-1}) for the 400-ha and 4000-ha facilities. Results represent the minimum annual averages for 21 years.

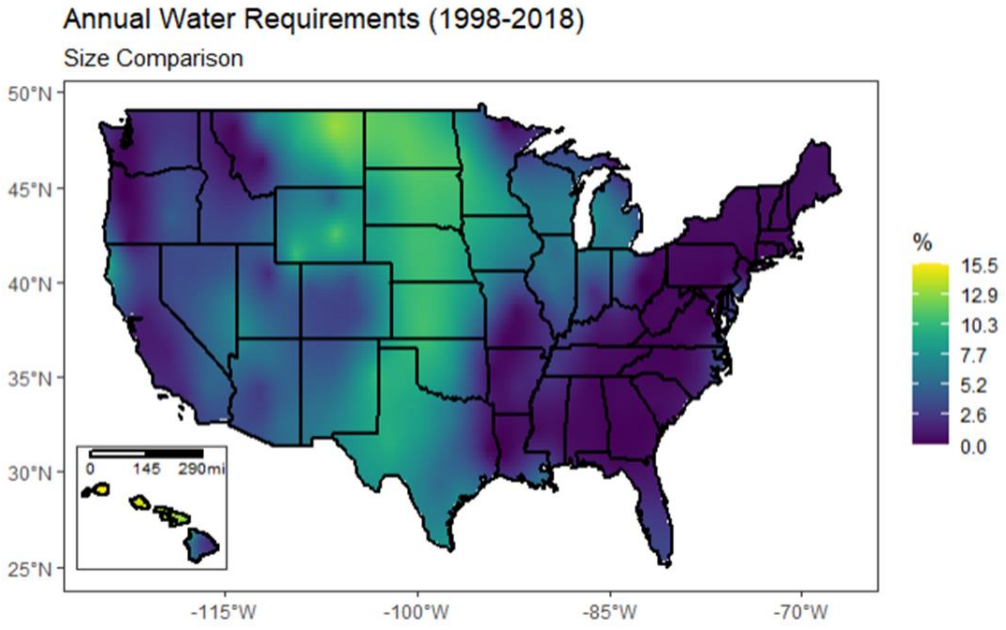

Figure A11. Comparison of the water demands of a 4000-ha to a 400-ha facility generated with weather data from the NSRDB. Results represent the absolute relative difference between annual averages.

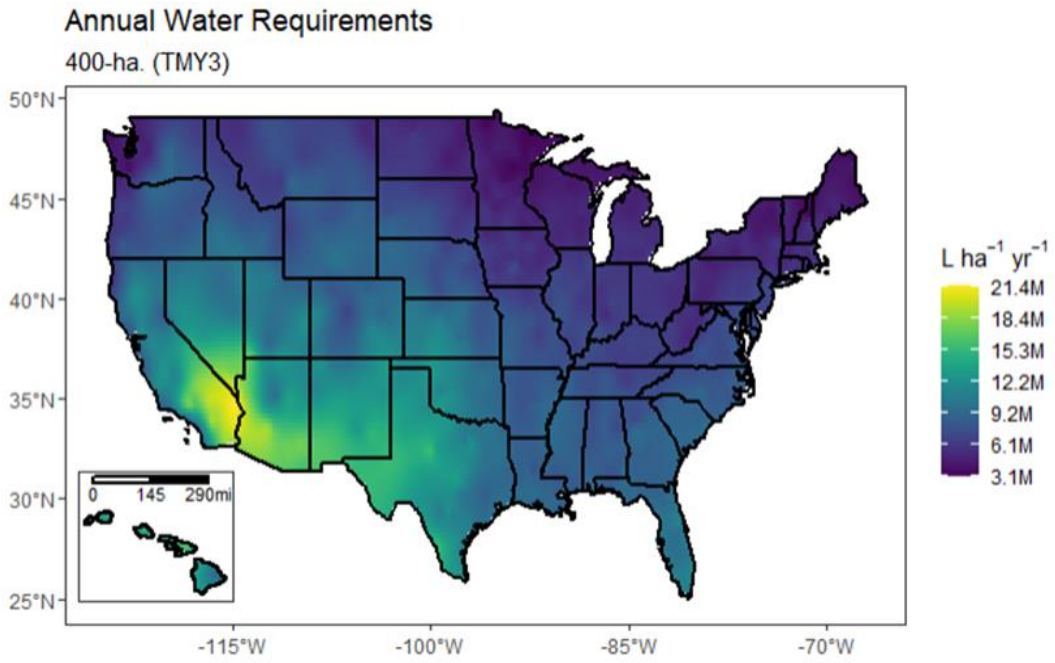

Figure A12. Annual water demands 3estimated with typical meteorological year (TMY3) data for a 400-ha algae farm.

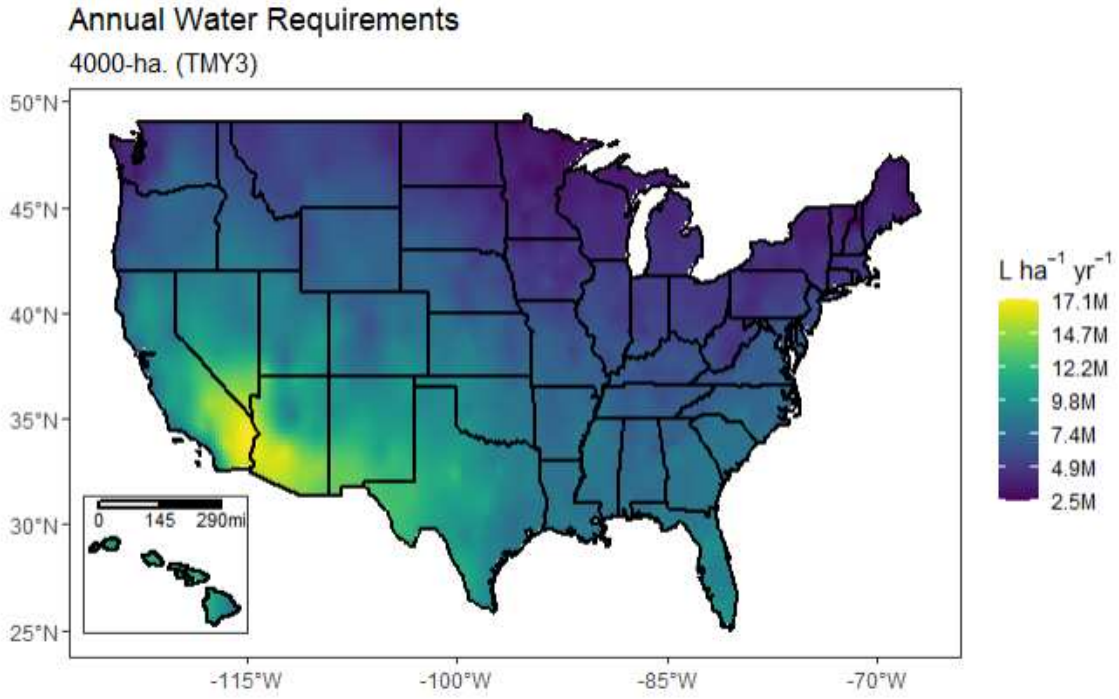

Figure A13. Annual water demands estimated with typical meteorological year (TMY3) data for a 4000-ha algae farm.

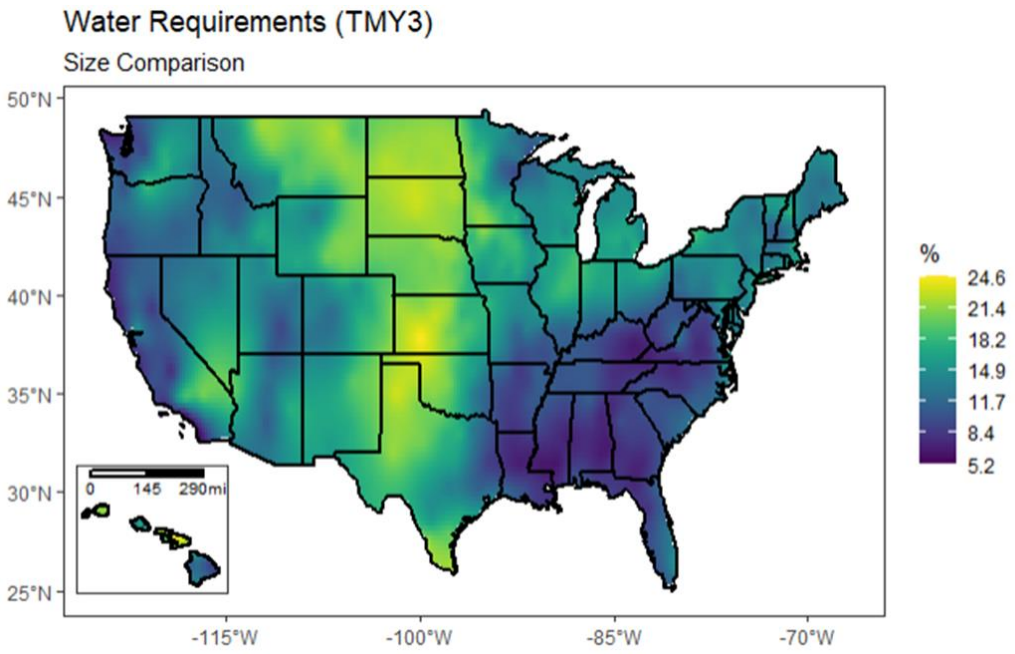

Figure A14. Comparison of the water demands of a 4000-ha to a 400-ha facility using TMY weather files.

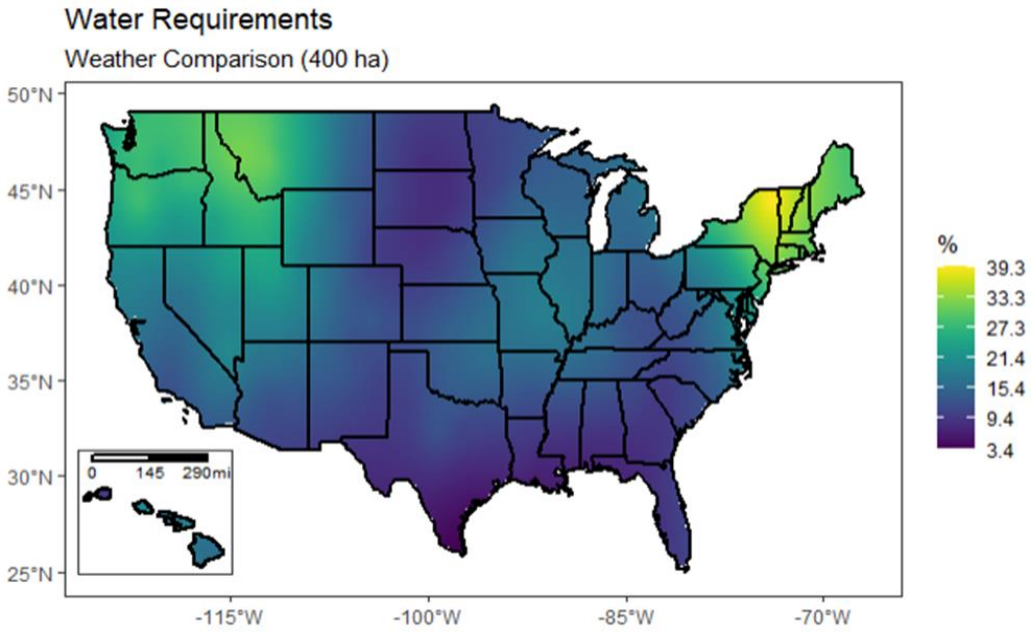

Figure A15. Comparison of the water demands generated with TMY3 weather data to results generated with weather data from the NSRDB (annual average 1998-2018). Water demands for a 400-ha facility are illustrated.

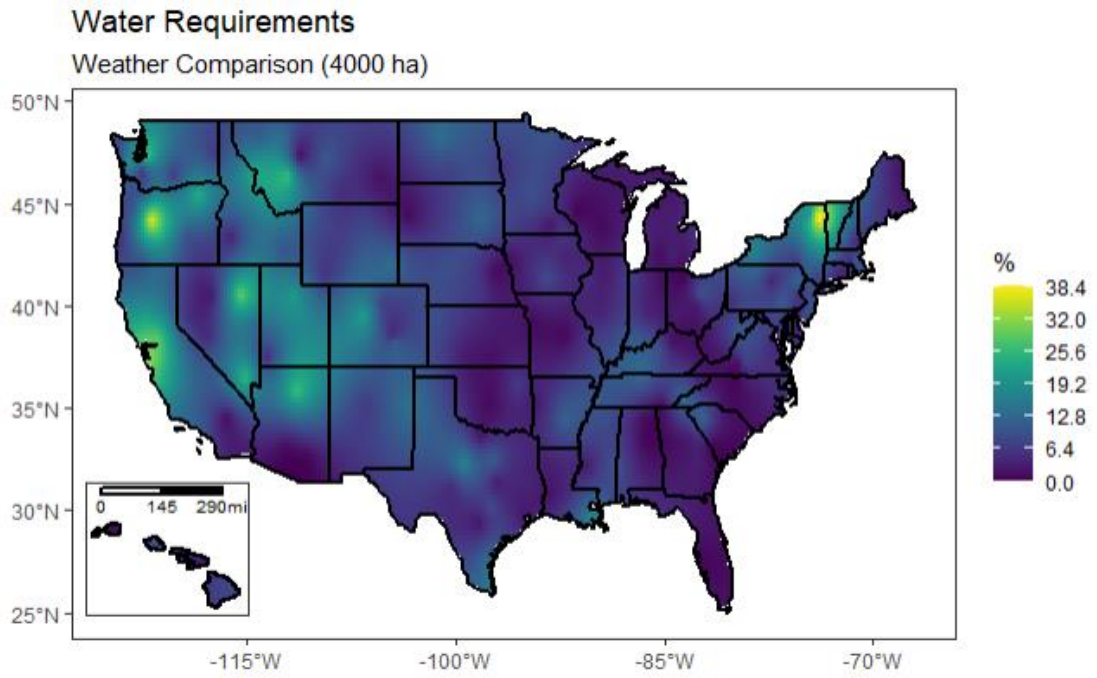

Figure A16. Comparison of the water demands generated with TMY3 weather data to results generated with weather data from the NSRDB (annual average 1998-2018). Water demands for a 4000-ha facility are illustrated.

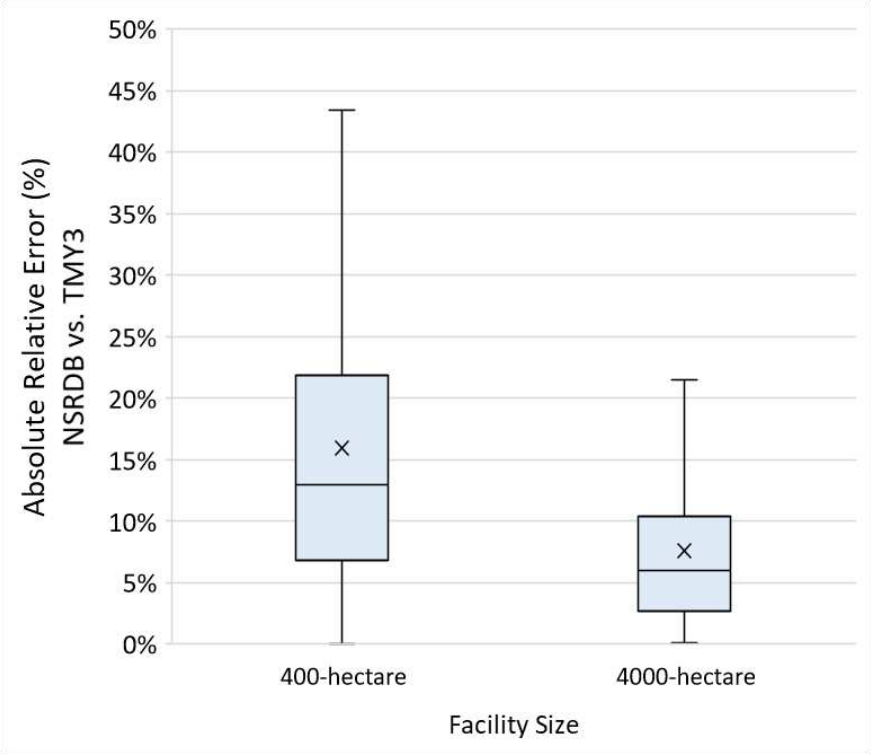

Figure A17. Absolute relative error between the water demands generated with TMY3 weather data to results generated with weather data from the NSRDB (annual average 1998-2018). Comparison for both facility sizes is shown, outliers are not shown.

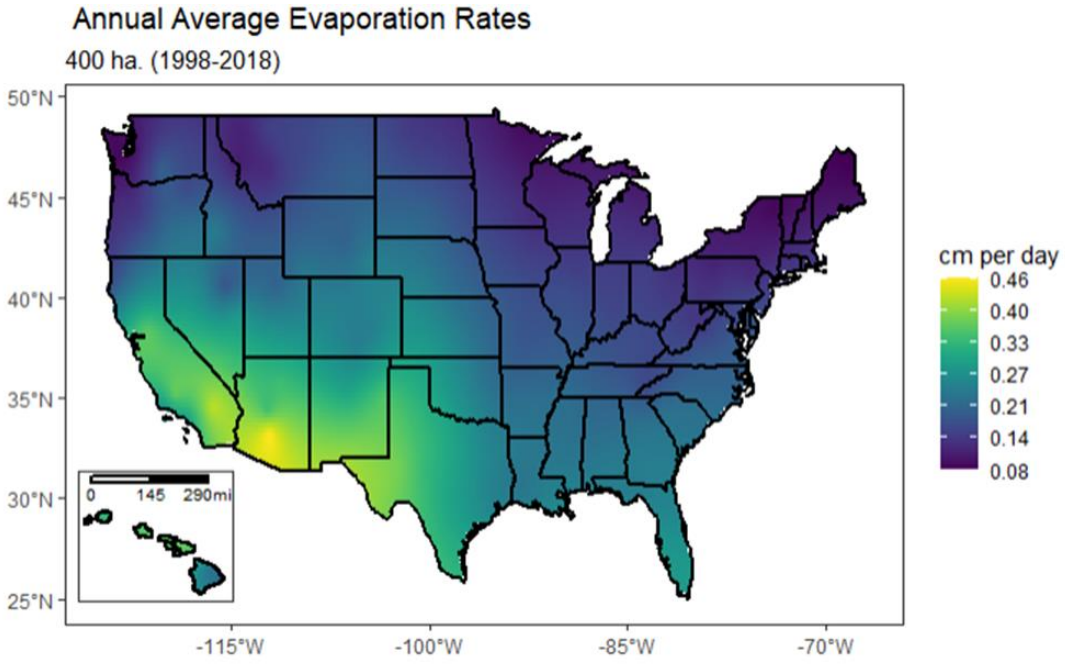

Figure A18. Mean annual water demand (cm day^{-1}) for a 400-ha algae farm. Results represent the average of 21 years.

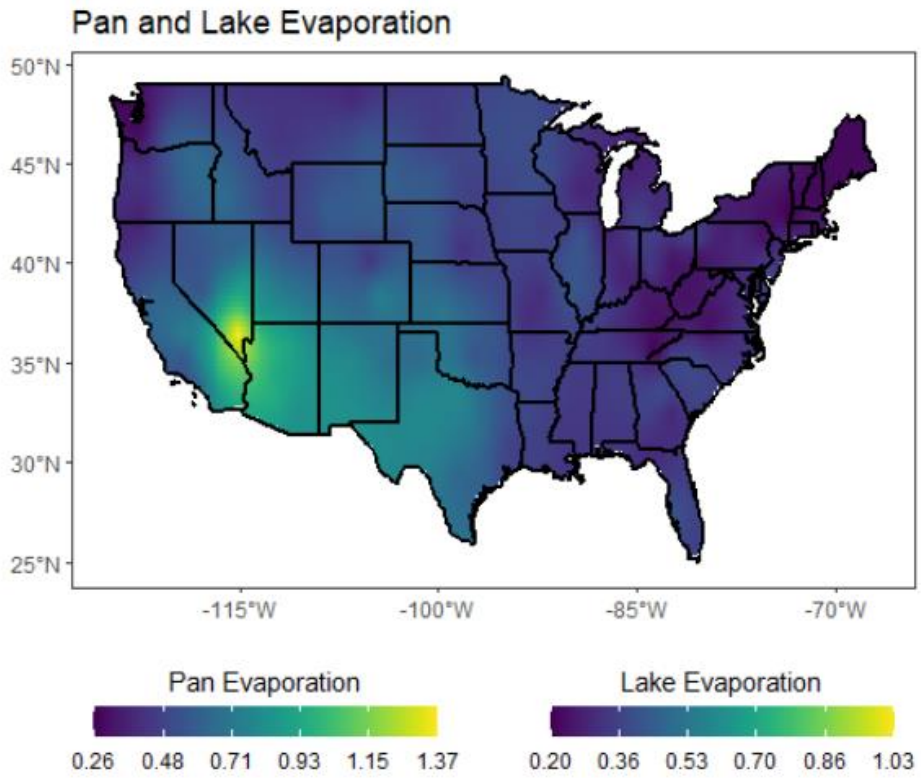

Figure A19. Mean annual water demand (cm day^{-1}) from pan evaporation measurements retrieved from Dewes et al. [10]. *Lake evaporation or corrected pan evaporation values were calculated by scaling pan measurements by 0.75.*

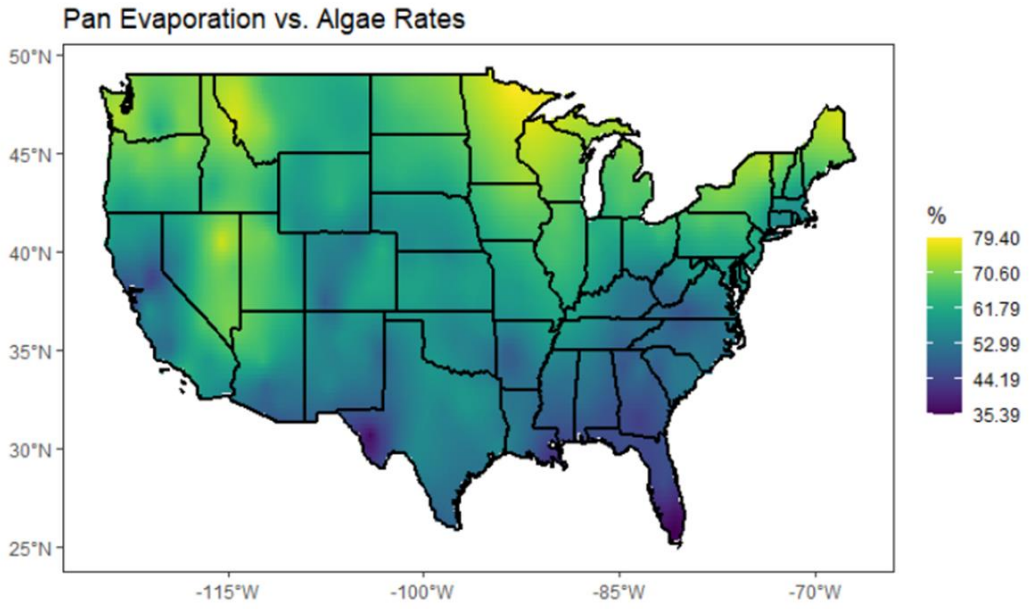

Figure A20. Comparison of the evaporation rates from pan evaporation to evaporation rates for an algal facility of 400-ha.

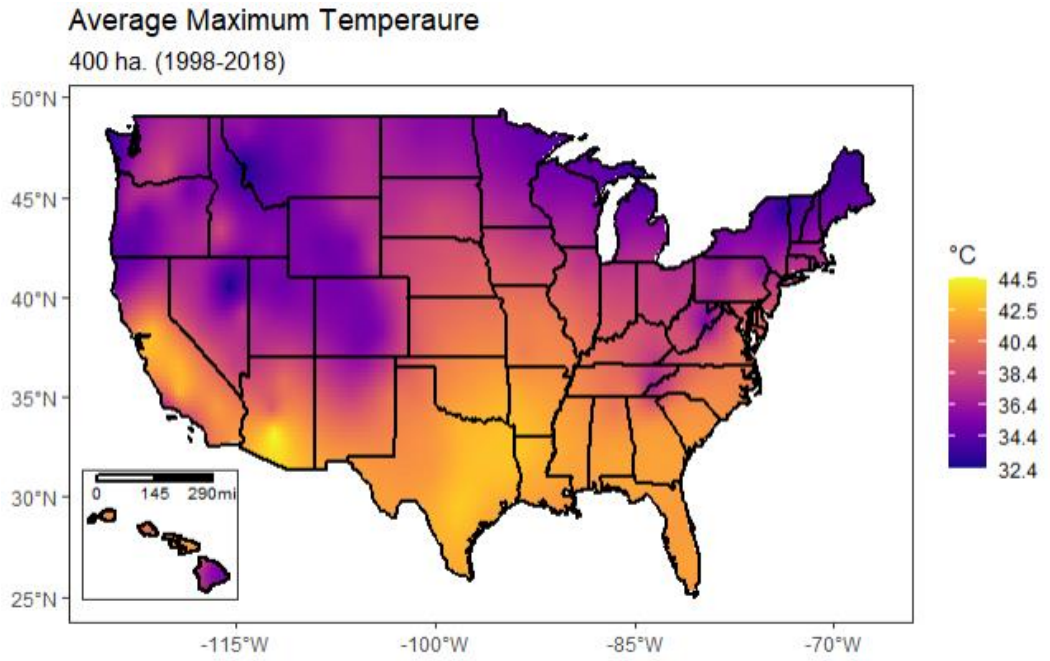

Figure A21. Mean annual maximum temperatures (°C) for a 400-ha facility, calculated using historical weather data.

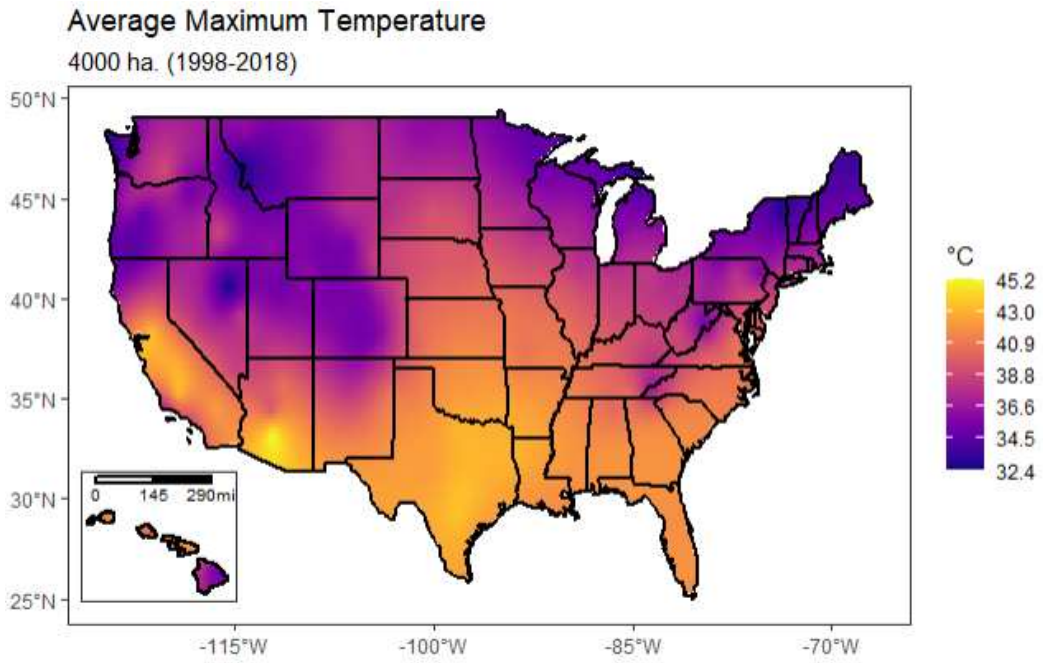

Figure A22. Mean annual maximum temperatures (°C) for a 400-ha facility, calculated using historical weather data.

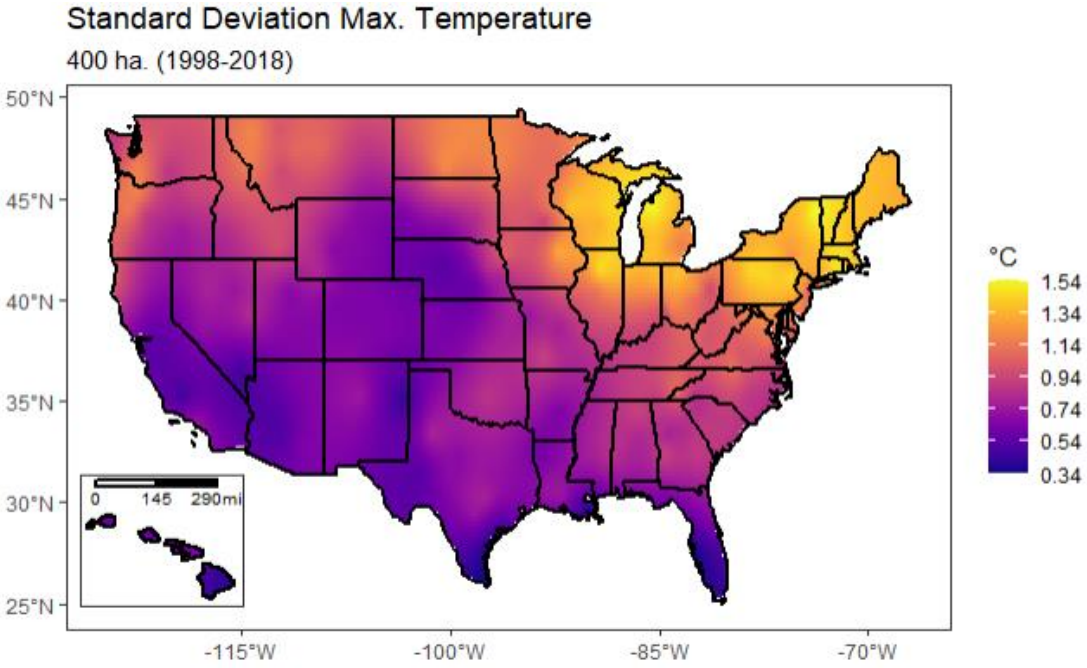

Figure A23. Standard deviation of annual maximum temperatures (°C) for a 400-ha facility, calculated using historical weather data from the NSRDB.

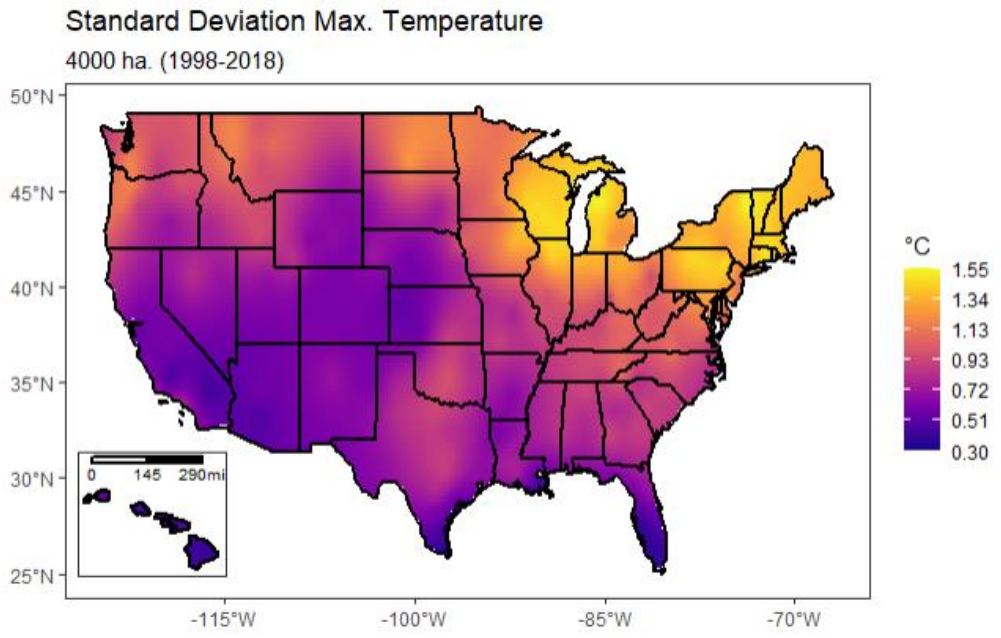

Figure A24. Standard deviation of annual maximum temperatures (°C) for a 400-ha facility, calculated using historical weather data from the NSRDB.

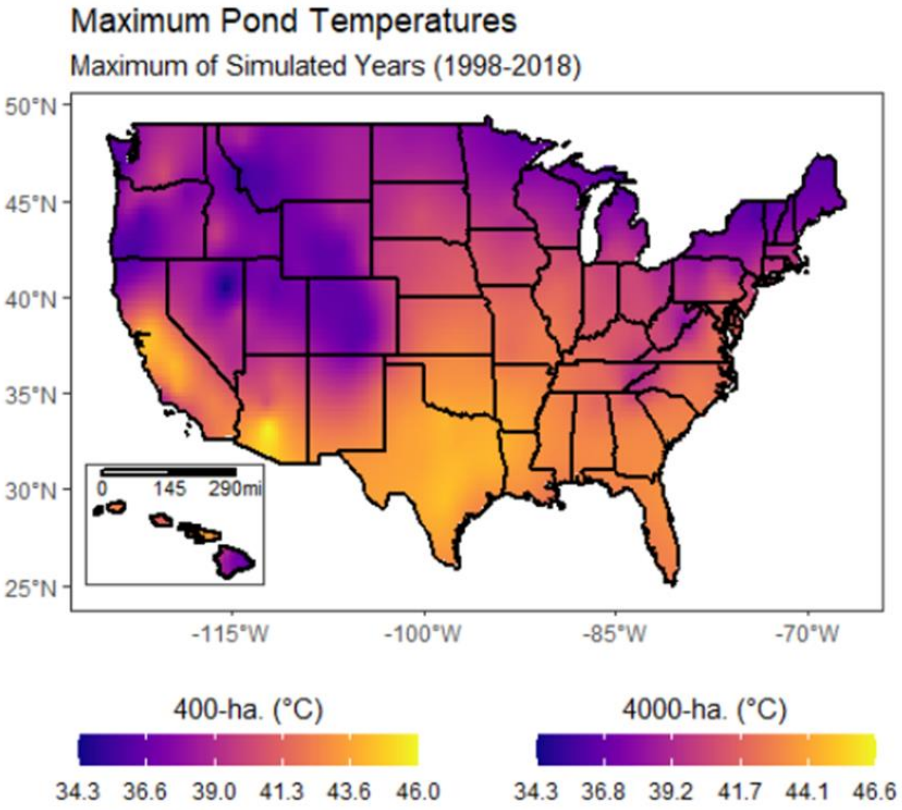

Figure A25. Maximum of annual maximum temperatures (°C) for both modeled facilities, calculated using historical weather data from the NSRDB.

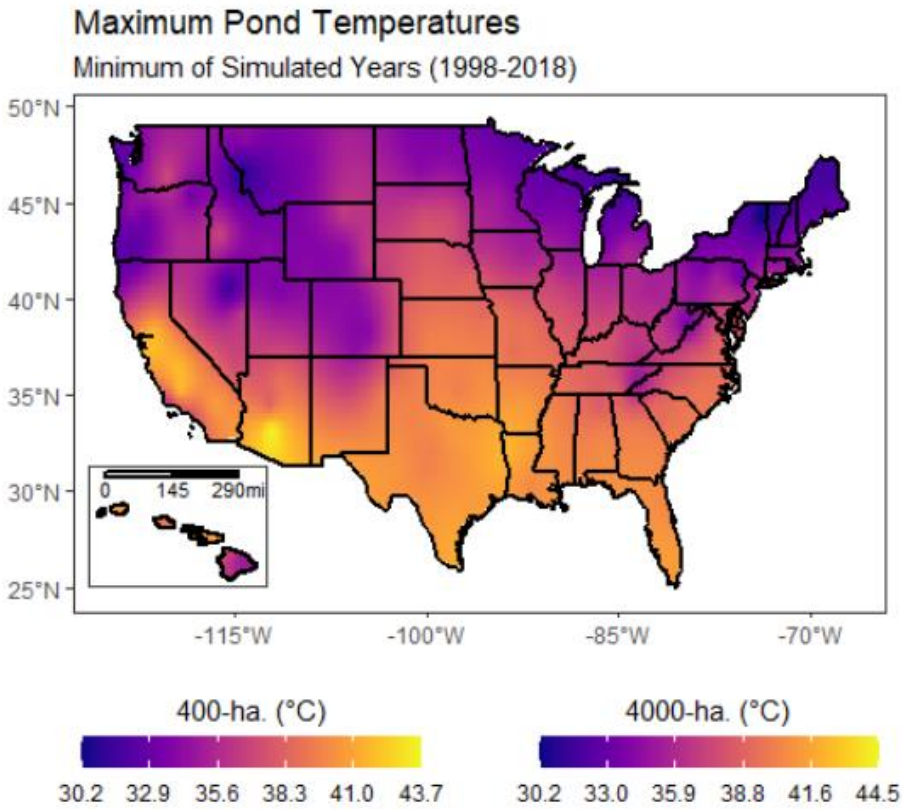

Figure A26. Minimum of annual maximum temperatures (°C) for both modeled facilities, calculated using historical weather data from the NSRDB.

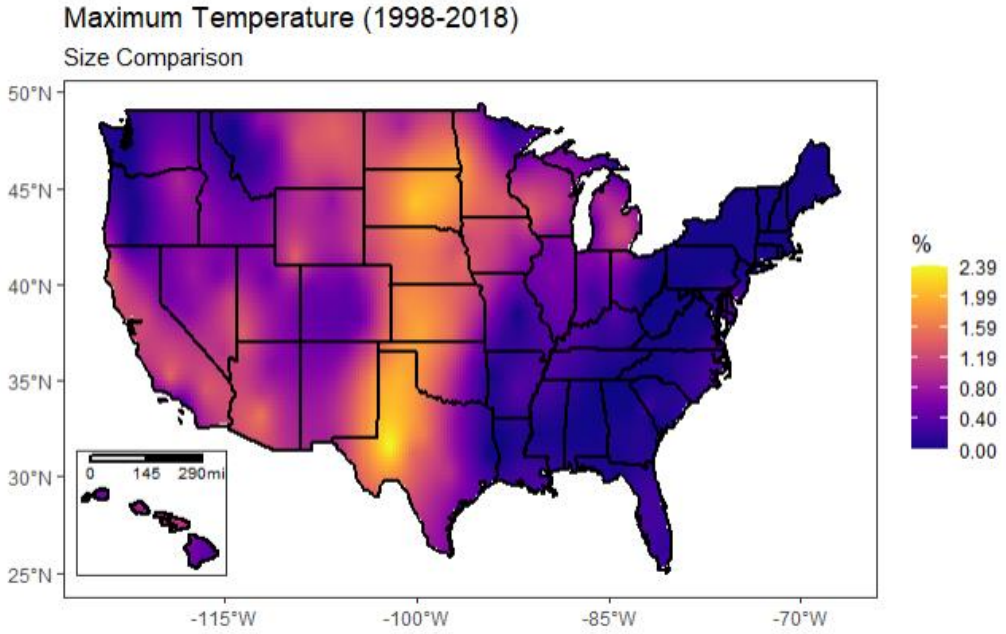

Figure A27. Mean maximum temperature comparison between a 400-ha and a 4000-ha facility. The mean of the total simulated period (21 years) for each location was compared.

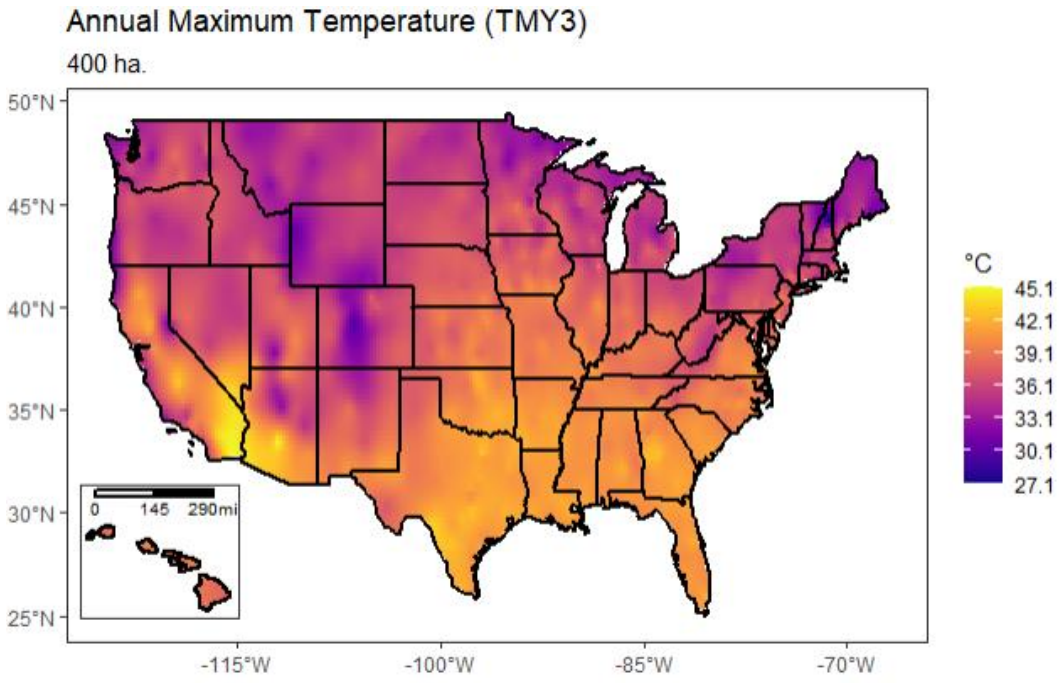

Figure A28. Maximum temperatures (°C) for a 400-ha, calculated with TMY data.

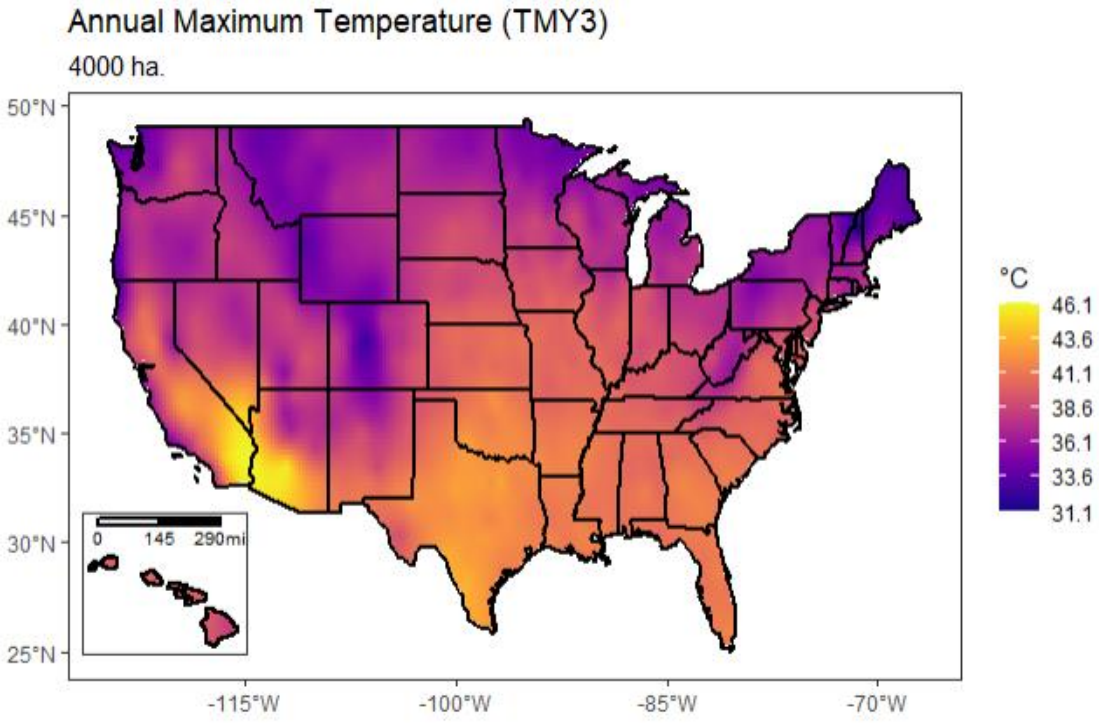

Figure A29. Maximum temperatures (°C) for a 4000-ha, calculated with TMY data.

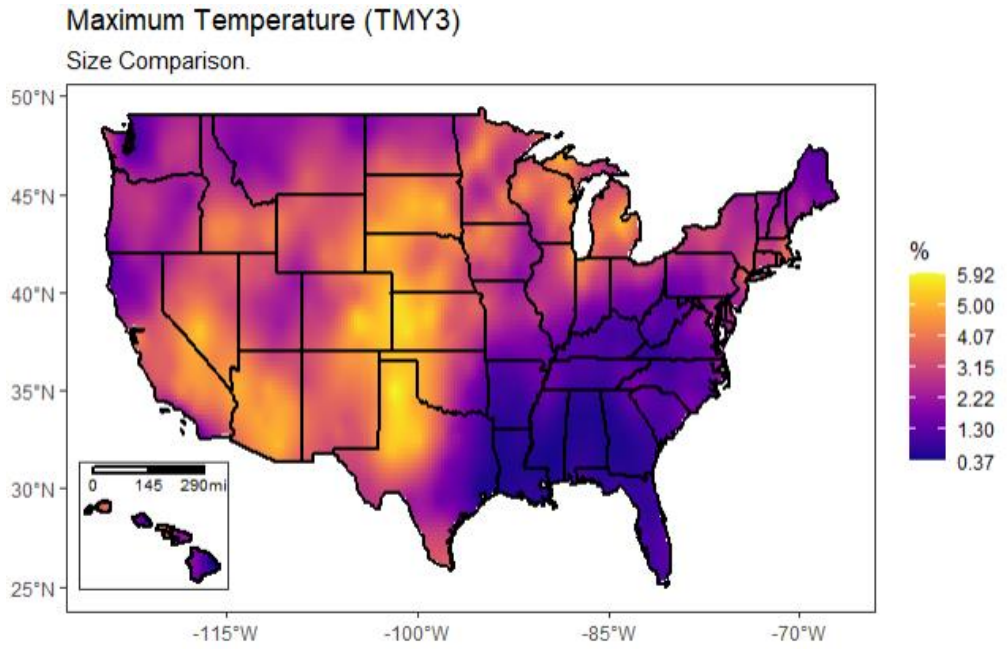

Figure A30. Comparison of the maximum temperatures reached on a 400-ha and 4000-ha facility using TMY data.

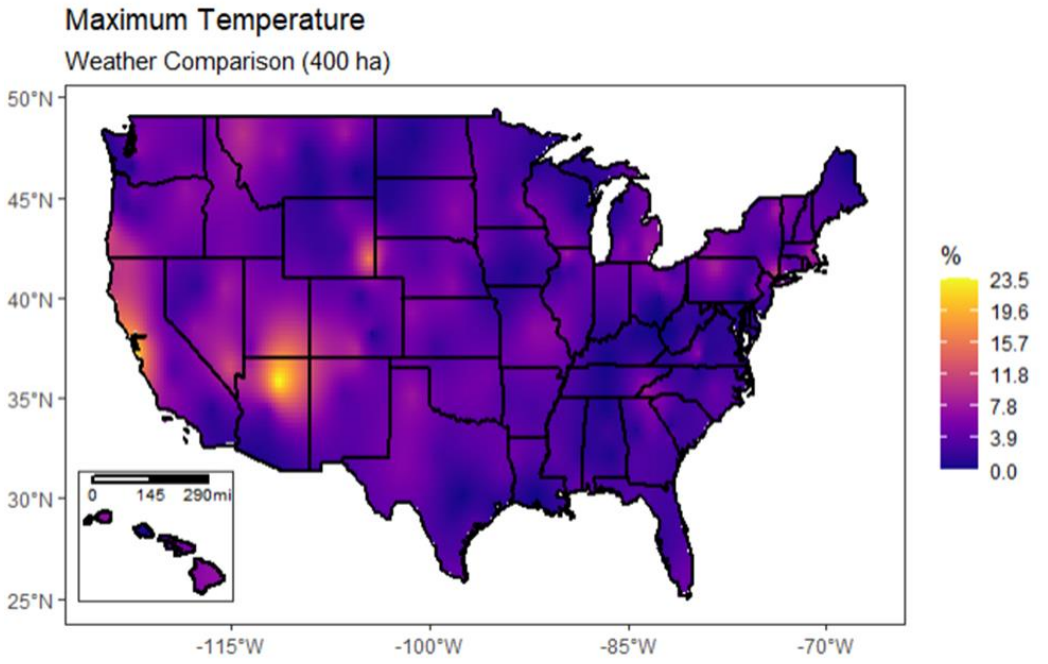

Figure A31. Comparison of the maximum temperatures calculated with historical weather data and TMY data. Results show temperatures for a 400-ha facility.

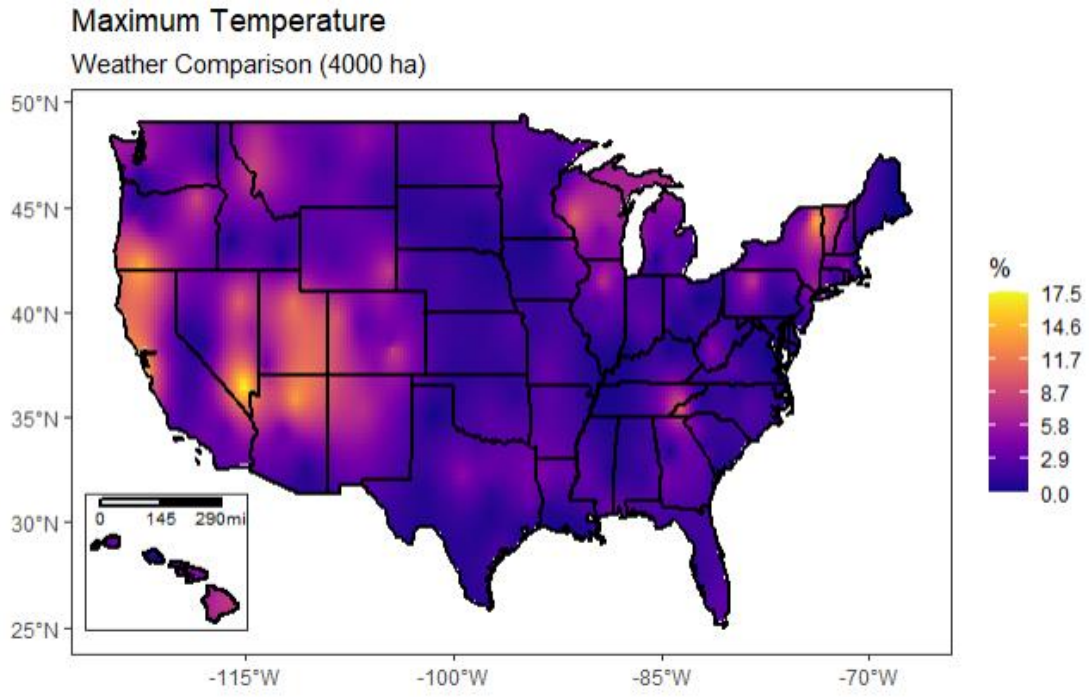

Figure A32. Comparison of the maximum temperatures calculated with historical weather data and TMY data. Results show temperatures for a 4000-ha facility.

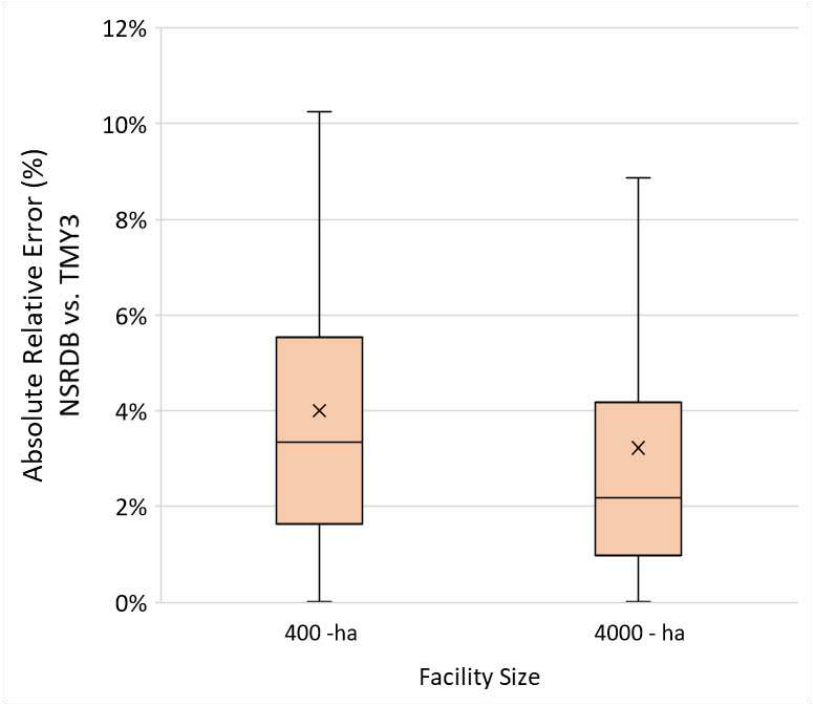

Figure A33. Absolute relative error between the maximum temperatures generated with TMY3 weather data to results generated with weather data from the NSRDB (annual average 1998-2018). Comparison for both facility sizes is shown, outliers are not shown.

A6. Dynamic maps of relevant weather inputs

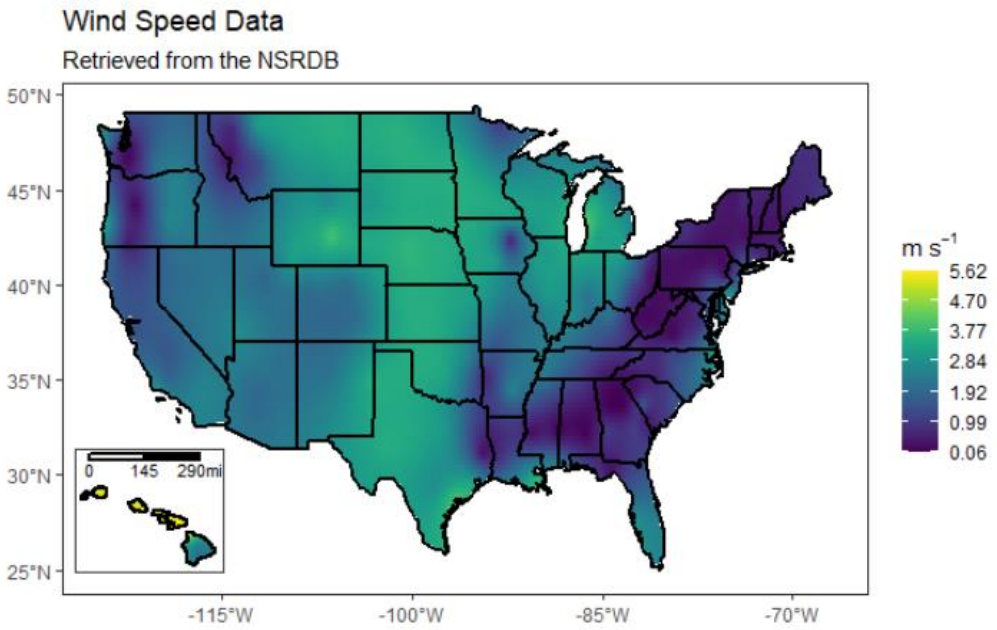

Figure A34. Average annual wind speed data (m s^{-1}) retrieved from the NSRDB. The average of 21 years is shown (1998-2018).

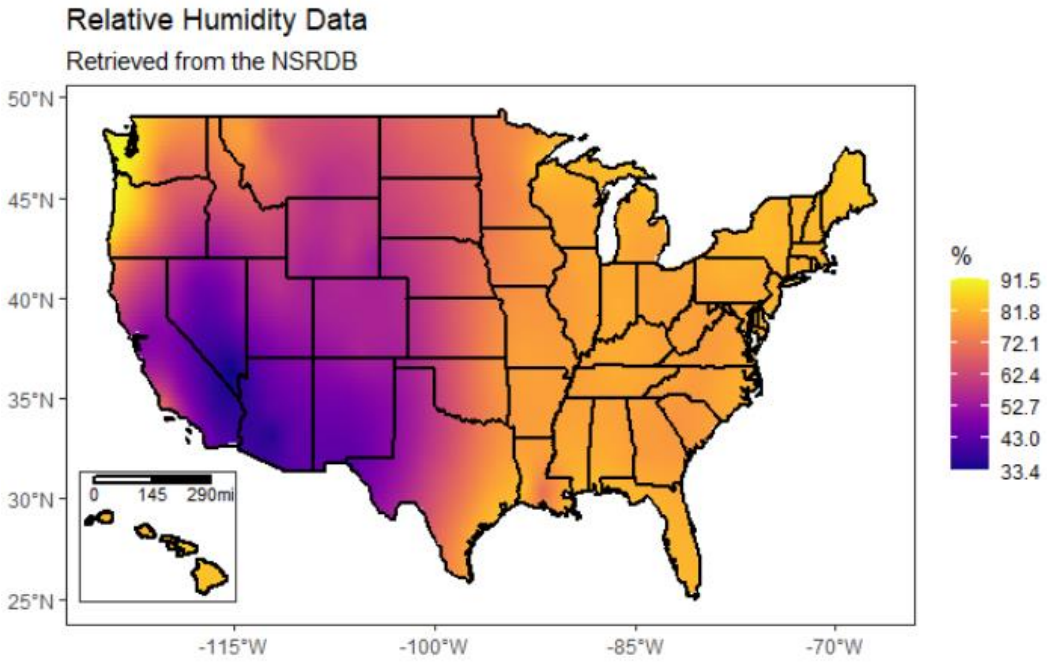

Figure A35. Average annual relative humidity data (%) retrieved from the NSRDB. The average of 21 years is shown (1998-2018).

A7. References

[1] J. C. Greene, Jonah M., Quiroz, David, Compton, Sam, Lammers, Peter J., Quinn, "A validated thermal and biological model for predicting algal productivity in large scale outdoor cultivation systems," *Algal Res.*, 2021.

[2] T. L. Bergman, A. S. Lavine, F. P. Incropera, and D. P. Dewitt, *Fundamentals of Heat and Mass Transfer*, 7th ed. John Wiley & Sons, Ltd, 2011

[3] M. E. Martínez, J. M. Jiménez, and F. El Yousfi, "Influence of phosphorus concentration and temperature on growth and phosphorus uptake by the microalga Scenedesmus obliquus," *Bioresour. Technol.*, vol. 67, no. 3, pp. 233–240, Mar. 1999

[4] P. W. Gerbens-Leenes, A. Y. Hoekstra, and T. H. Van Der Meer, "The water footprint of bio-energy: Global Water Use for Bio-Ethanol, Bio-Diesel, Heat and Electricity," *Value Water Res. Rep. Ser.*, vol. 34, no. 34, p. 108, 2008

[5] a K. Chapagain and a Y. Hoekstra, "Water Footprints of Nations (Vol 2)," *Water Res.*, vol. 2, no. 16, p. 240, 2004.

[6] F. W. T. Penning De Vries, D. M. Jansen, H. F. M. Ten Berge, and A. Bakema, "Simulation of ecophysiological processes of growth in several annual crops."

[7] B. E. Dale, "Biomass Refining: Protein and Ethanol from Alfalfa," *Ind. Eng. Chem. Prod. Res. Dev.*, vol. 22, no. 3, pp. 466–472, 1983.

[8] R. J. Henry, "THE CARBOHYDRATES OF BARLEY GRAINS - A REVIEW," *J. Inst. Brew.*, vol. 94, no. 2, pp. 71–78, Mar. 1988.

[9] a K. Chapagain and a Y. Hoekstra, "Water Footprints of Nations (Vol 2)," *Water Res.*, vol. 2, no. 16, p. 240, 2004.

[10] C. F. Dewes, I. Rangwala, J. J. Barsugli, M. T. Hobbins, and S. Kumar, "Drought risk assessment under climate change is sensitive to methodological choices for the estimation of evaporative demand," *PLoS One*, vol. 12, no. 3, p. e0174045, Mar. 2017.